Volume 5, Issue 2, 2019

Journal of Biomedical Photonics & Engineering

Special Issue

"Laser and optical technologies in biomedicine and ecology"

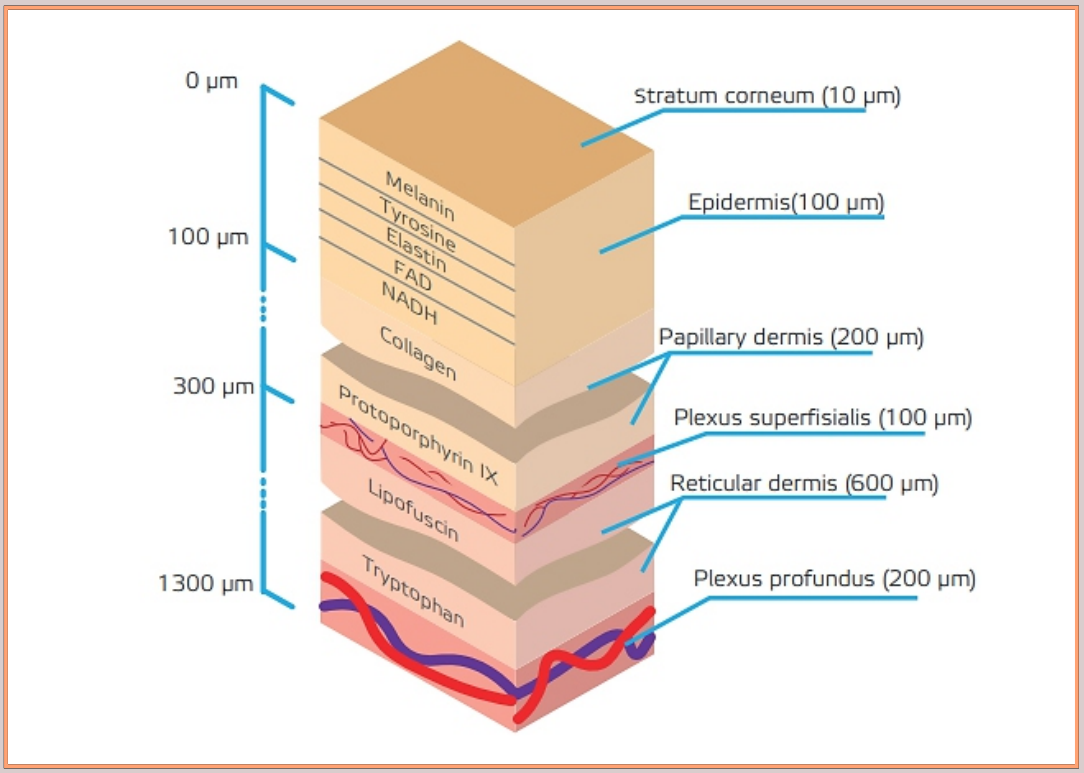

Special Issue Editors:
Aleksandra M. Mayorova and Ivan A. Bratchenko

 doi: 10.18287/JBPE18.05.020001

Journal of Biomedical Photonics & Engineering

by Samara National Research University

Volume 5, Issue 2 (June 2019)

Editorial Board

Postal address:
39B Lukacheva st., room #301
Samara 443086, Russian Federation

doi: 10.18287/JBPE18.05.020001

Special Issue
“Laser and optical technologies in biomedicine and ecology”

Special Issue Editors

Aleksandra M. Mayorova
Samara Branch of P.N. Lebedev Physical Institute of Russian Academy of Sciences

Ivan A. Bratchenko
Samara National Research University

Used Figure from this issue on the Cover

Anastasia O. Ustinova et al. Monte Carlo simulation of skin multispectral autofluorescence, 020306, Fig. 1.

Contents

 doi: 10.18287/JBPE18.05.020101

Foreword to the Special Issue on Laser and optical technologies in biomedicine and ecology

Dear Colleagues,

It is our pleasure to present you the Special Issue of the Journal of Biomedical Photonics & Engineering (J-BPE) with selected papers of the Biophotonics Workshop of the XVI All-Russian Youth Samara Conference-Contest on Optics and Laser Physics (Samara, November 13-17, 2018). The conference-contest was organized by P.N. Lebedev Physical Institute (Samara Branch) and Samara National Research University and supported by Russian Foundation for Basic Research (grant No. 18-32-10033), Administration of Samara Region and Samara SPIE Student Chapter.

The Biophotonics Workshop is one of the most interesting workshops of the Conference. The papers presented in the Special Issue of J-BPE cover a broad range of topics on applications of laser and optical techniques for solving of biomedical problems.

In their study, **Anna Neupokoeva** and co-authors from Irkutsk State Medical University and Irkutsk Technical National University analyzed the changes of an insulin solution's structure under the influence of 650 nm laser radiation. The researchers used nanometer resolution probe microscope for analyses of insulin crystallograms. Also they performed correlation processing of speckle patterns obtained by passing laser radiation through the solution. It was shown that laser radiation promoted solution homogenization. So the authors believe that the laser effect is important for improving insulin effectiveness in the body and reducing insulin consumption.

The aim of the paper of **Lubov Kokorina** and **Anna Neupokoeva** (Irkutsk State Medical University) was to investigate the effect of laser irradiation on the activity of plant pharmaceuticals. In particular, the authors supposed that laser radiation facilitated destruction of the solutions clusters into components and thus would increase the biochemical activity of the drugs. They observed the different bacteria growth dynamics for pre-irradiated and non-irradiated pharmaceuticals.

Kristina Ganichkina and co-authors (Samara National Research University) experimentally studied the properties of porous silicon as well as nanocomposites on its base with hydroxyapatite. The authors analyzed IR spectra of material samples with glucose and hydroxyapatite. They concluded that porous silicon is promising material for glucose biosensors. And also the researchers believe that nanocomposites porous silicon - hydroxyapatite suitable biomaterial for osteoplasty.

Various silicon nanostructures, for example nanowires, mesoporous nanoparticles and others, obtained by plasma-chemical synthesis and laser-ablation methods were investigated by **Alida Alykova** and co-authors from National Research Nuclear University MEPhI, Lomonosov Moscow State University and Lebedev Physical Institute. On the base of Raman spectra, the researchers studied the dissolution in water of various types of particles. Depending on the rates of dissolution

 doi: 10.18287/JBPE18.05.020101

they gave recommendations for the use of each type of nanoparticle for specific biomedical applications.

The team of researchers from Saratov State University, Tomsk State University, Saratov State Medical University, Institute of Precision Mechanics and Control RAS, ITMO University and Samara National Research University **Ekaterina Lazareva** and others presented the development of multi-wavelength refractometric technique for estimating the degree of skin dehydration when using optical clearing agents such as glycerol and glucose. The researchers conducted *in vitro* and *in vivo* measurements in the visible and NIR spectral regions. They demonstrated the differences in the dehydration of healthy skin and skin with tumor. Thus the developed technique is promising as a new diagnostic and monitoring method for oncological diseases.

Ananstasia Ustinova, **Ivan Bratchenko**, and **Dmitry Artemyev** (Samara National Research University) suggested six-level skin model for the Monte Carlo simulation of human skin autofluorescence in different spectral ranges. Detailed analyze of literature data allowed the authors to identify some main fluorophores for every skin layer and on the base of known values of their absorption and scattering coefficients as well as fluorescence properties simulate the fluorescence spectra exited by radiation at different spectral regions. The authors compared their model autofluorescence spectra with experimental data obtained by other researchers. They concluded that the proposed model of human skin autofluorescence is correct enough to use in further studies.

Thus, the collected papers of the Special Issue demonstrate potential of optical and laser technologies and also the application of nanomaterials in different biomedical studies and applications.

Special Issue Editors:

Aleksandra M. Mayorova
Samara Branch of P.N. Lebedev Physical Institute of Russian Academy of Sciences
E-mail: mayorovaal@gmail.com

Ivan A. Bratchenko
Samara National Research University
E-mail: iabratchenko@gmail.com

Laser photomodification of insulin solution

Anna V. Neupokoeva[1*], Evgenia A. Kuzina[1], Nikita S. Moskalev[1], Anna I. Nikonova[1], and Sergey A. Nebogin[2]

[1] Department of Medical and Biological Physics, Irkutsk State Medical University, 1 Krasnogo Vosstaniya St, Irkutsk 664009, Russia

[2] Department of Quantum Physics and Nanotechnology, Irkutsk National Research Technical University, 83 Lermontov St., Irkutsk 664074, Russia

*** e-mail:** annett_2005@inbox.ru

Abstract. The article discusses influence of laser radiation on structure of insulin solution. We monitored changes in the structure of insulin solutions by means of analysis of crystallograms with a nanometer resolution probe microscope as well as by correlation processing of speckle patterns obtained by passing laser radiation through the solution. It was experimentally shown that laser radiation promoted solution homogenization by changing size of macromolecular clusters. © 2019 Journal of Biomedical Photonics & Engineering.

Keywords: crystallogram; image processing; structure monitoring; laser biostimulation.

Paper #3314 received 10 Feb 2019; revised manuscript received 18 Mar 2019; accepted for publication 15 Apr 2019; published online 13 May 2019. doi: 10.18287/JBPE19.05.020301.

1 Introduction

Laser radiation has been used in medicine for several decades and currently has a number of methods differing time and location of exposure, wavelength and radiation power [1]. At the same time, there is no generally accepted theory explaining mechanisms of laser therapy. But ways of detecting changes that occur under action of laser radiation recently have significantly expanded. Thus, different experimental techniques of structural changes of complex organic solutions such as Raman spectroscopy and IR spectroscopy, crystallographic method and method of speckle patterns processing have become widespread in practice [2–8]. Using new research methods has led to appearance of some new theories about the mechanisms of action of laser radiation on living organisms [1, 4, 9, 10]. In particular, in Ref. [4] primary action of laser radiation was considered as a result of interaction with blood proteins. In Ref. [10] the authors supposed that laser radiation reduced macromolecular clusters that formed protein molecules in water solution and thus changed their functional activity. In addition, in article [10] it was shown that laser radiation could affect molecular clusters not only in biological fluids, but also in drugs composition that leads to increasing their effectiveness.

Therefore, the purpose of this work is to study effect of laser radiation on the microstructure of an insulin solution. The choice of the object of research was due to two main reasons. First, it is nature of an insulin molecule formed by two polypeptide chains, which contains 51 amino acid residues. Six insulin molecules are bound in a hexamer. Molecules are hold together by histidine residues bound by zinc ions. Injected insulin is under the skin in the form of a hexamer, which gradually breaks down into biologically active monomers that enter the bloodstream. Secondly, according to the World Health Organization, the number of diabetics is more than 3% of the world's population. Moreover, a significant percentage of these patients are forced to take daily drugs (in particular, insulin) to decreasing their blood glucose levels. Therefore, it is important to develop methods aimed at improving insulin effectiveness in the body and reducing insulin consumption.

2 Materials and methods

The method of crystallogram analysis was used for adequate assessment of structural changes occurring under action of laser radiation in biosimilar liquids as one of the simplest methods of structural changes diagnostics. Crystallograms of biological fluids were formed due to dehydration self-organization of protein solutions and other substances [6, 11] during drying of solution droplets on a solid substrate. It was found that the resulting patterns correlate well with the signs of

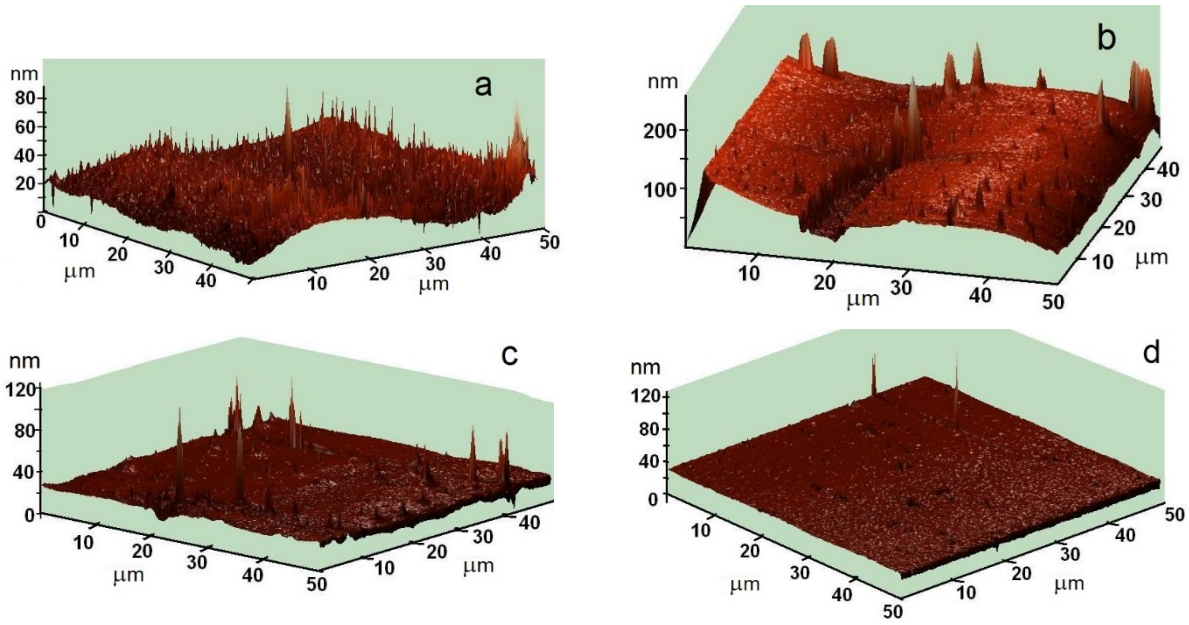

Fig. 1 3D model of the insulin solution crystallogram surface: a – control (before exposure), b – after 5 minutes, c – after 10 minutes, d – after 15 minutes.

patients' diseases [6, 12, 13]. Therefore, the method of crystallogram analysis can be used to record changes occurring in biological fluids under laser radiation exposure. The detecting capability of laser-induced changes in serum and plasma was shown in Ref. [5]. A possible mechanism of laser-induced changes is decreasing bioorganic molecules (primarily macromolecules) clusters size under the influence of laser radiation [5].

Usually crystallogram analysis is carried out by an optical microscope. In this case the geometric dimensions (longitudinal and transverse) of the characteristic structures of the crystallogram are estimated, while information about the relief (surface profile) is usually lost. That is why, in this paper the analysis of crystallograms was carried out by a probe microscope to obtain information about three-dimensional structure of the crystallogram.

As an alternative method of changes recording in the microstructure of the protein solution, the "chessboard" method for speckle patterns processing was chosen. Since protein clusters in the solution form optical inhomogeneities, when laser radiation passes through a cell with such solution, a speckle pattern is formed, and a characteristic speckle size depends inversely on the inhomogeneity (cluster). To determine the characteristic speckle size, the correlation coefficient of a two-dimensional speckle image and a regular structure ("chessboard") was calculated. Paper [14] presents a program that calculates the correlation coefficient of a speckle image and "chessboards" with various sizes from 5×5 to 100×100 pixels in 5 pixel increments until the most clearly expressed structure is obtained. The chessboard, with the most clear structure and the biggest correlation coefficient was taken as a standard. Then every speckle image was analysed with this standard: the correlation coefficient of the reference image and each of the analyzed images was calculated.

The research object was a solution of human insulin in the form of the drug "Actrapid" in ampoules. The insulin solution was poured into a cuvette and exposed by laser irradiation with a wavelength of 655 nm and intensity 150 mW/cm^2. The exposure time was 2, 5, 10, 15 minutes. Before irradiation, a control (non-exposed) sample was poured onto the glass plate. Then, after each irradiation time, several drops of the solution were also poured onto a glass substrate. All samples were kept at room temperature to obtain crystallograms. Crystallogram of the insulin solution is a thin transparent film with inhomogeneities invisible not only by naked eye, but also by an optical microscope. Therefore, the obtained crystallograms were investigated in a scanning probe microscope NT-MDT solver (contact scanning method).

3 Results

3D models of crystallogram relief (Fig. 1) were built using a probe microscope. The increasing time of laser exposure caused significant decreasing the number of crystallogram peaks and average peak height and increased the layer smoothness. So, before exposure, the average height of the peak was 50–60 nm, and the maximum – about 80 nm. After 5- and 10-minute exposure, the peak height did not change significantly, but their frequency went down significantly: from 60-80 to 100 μm^2 in the control, to 5–8 per 100 μm^2 after 10 minutes of radiation. After 15-minute exposure the average peak height became 30 nm and peak frequency reduced to 3–4 per 100 μm^2.

A significant increasing the smoothness of crystallogram layer was caused by the conformational

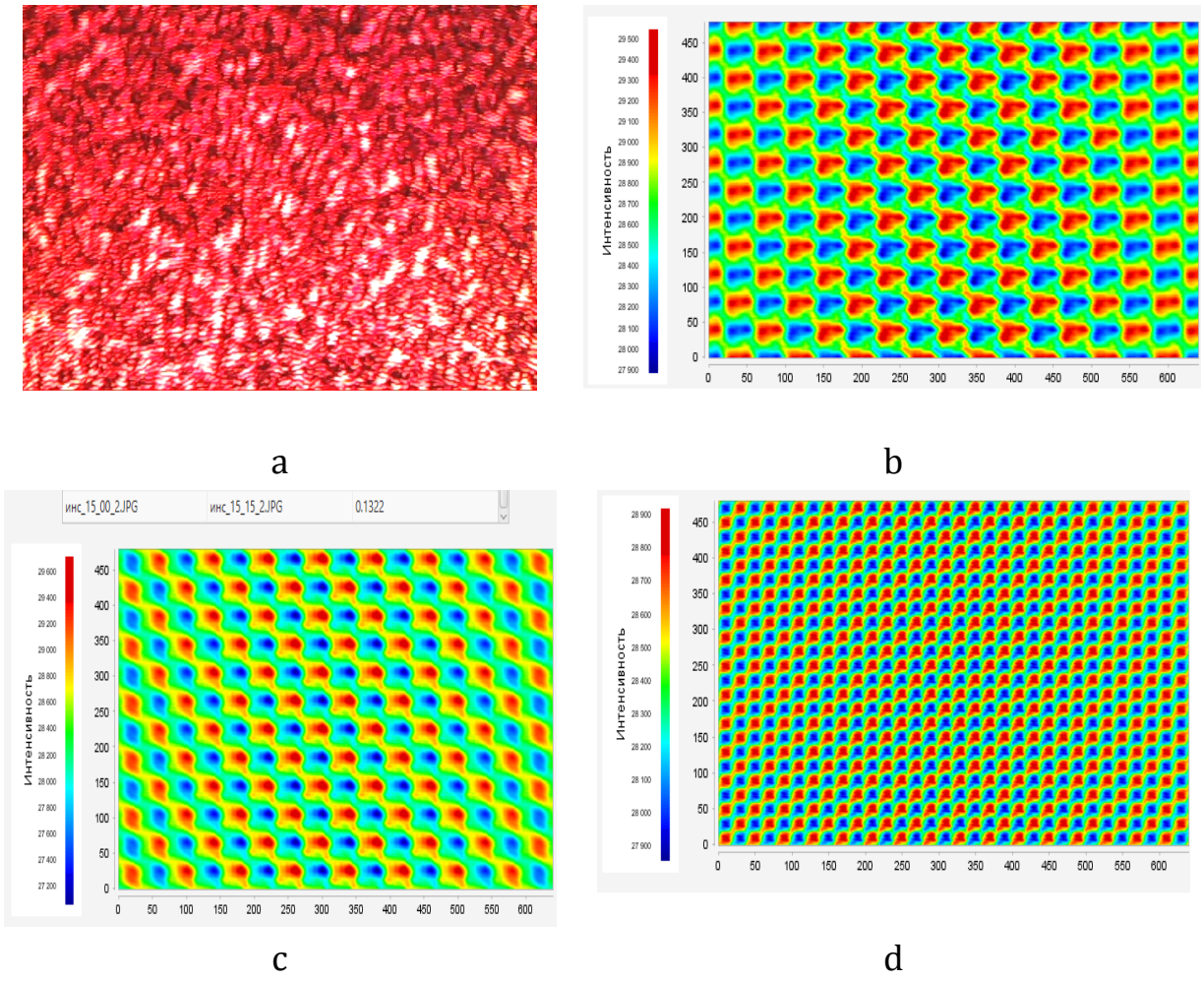

Fig. 2 A characteristic type of speckle pattern from the control sample (a), the correlation fields of the reference chessboard (40×40 pixels) and the control speckle pattern (b), and the speckle pattern obtained after 15 minutes of laser exposure (c), the correlation field of the chessboard 20×20 pixels and the speckle pattern obtained after 15 minutes of laser exposure (d). Counts in pixels are situated on the vertical and horizontal axis of the correlation field, theamplitude of the correlation coefficient at each point of the field is indicated by color.

state changes of protein molecules in the solution. Before laser exposure, organic macromolecules in solution had an aqueous environment and formed clusters of different sizes and configurations: from very large to very small. During solution drying macromolecular clusters of large sizes (which as a whole had a lower rate of chaotic motion) were fixed on the substrate the first and they played the role of crystallization centers for the crystal growth in the film. Then smaller associates were deposited and, at the end, the smallest, that formed peaks due to the fact that their small mass allowed to stay on the top of the resulting peak.

After laser exposure the solution was homogenized: large clusters were divided into smaller ones, and the smallest clusters merged, became larger. Thus, the degree of cluster size variation decreased. During crystallization from a solution homogenized after laser exposure, the associates were placed in a smoother layer, since the share of minimum size clusters forming peaks decreased, and the number of peaks decreased too.

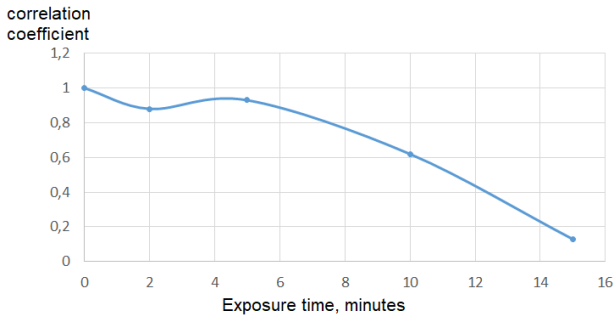

Fig. 3 The dependence correlation coefficient of the reference chessboard and speckle-patterns obtained at different time points.

Characteristic type of speckle pattern from the control sample, correlation fields between the reference chessboard (40×40 pixels) and the control speckle

pattern and the speckle pattern obtained after 15 minutes of laser exposure are presented in Fig. 2. The correlation field of the speckle pattern obtained before irradiation had a clearly defined peak, while the correlation field of the speckle pattern obtained after 15 minutes of exposure had a peak with smaller amplitude and more blurred shape, which led to the characteristic maxima chains formation. It means that the characteristic speckle size did not match the square size on the "chessboard". For comparison, the correlation field of the speckle pattern obtained after 15 minutes of irradiation and a chessboard with a square size of 20×20 pixels are presented in Fig. 2(d). This field shows a set of clearly defined peaks, which indicates the equality of the chessboard squares (20×20 pixels) and speckle size. Thus, it can be argued that the characteristic size of the speckle varies from 40 to 20 pixels (or from 15 to 30 microns), which corresponds to the inhomogeneity size increasing by 2 times in the solution. In addition, the obtained result can be interpreted as the cluster size spread decreasing, with an increasing of the large clusters contribution to the speckle pattern formation.

There is correlation coefficient dependence of the reference checkerboard (40×40 pixels) and the speckle patterns obtained at different time points in Fig. 3. A decreasing of the correlation coefficient between the speckle pattern and the reference chessboard also indicates a changing of the characteristic speckle size. While the speckle size remained approximately equal to the square size of the "chessboard", the correlation coefficient had high values (0.8–1). After 5 minutes of laser exposure the microstructure of the insulin solution was modified, that caused the characteristic speckle size decreasing and this size became not equal to the chessboard square size and it led to a sharp reducing of the correlation coefficient.

4 Conclusion

It was shown experimentally that the insulin solution structure changed under action of 655 nm laser radiation. Analysis of insulin crystallograms with the help of probe microscope revealed a significant increase of surface smoothness due to irradiation. We supposed that laser exposure of the insulin solution caused such conformational changes which led to greater cluster size homogeneity in the solution. At the same time, the contribution of large clusters to the formation of speckle pattern increased, that led to a twofold reduction in the characteristic speckle size: from 40 to 20 pixels (which corresponded to a change in cluster size from 15 to 30 μm).

Disclosures

All authors declare that there is no conflict of interests in this paper.

References

1. A. V. Kartelishev, A. G. Rumyancev, A. R. Evstigneev, A. V. Geiniz, and S. V. Usova (Eds.), Lazernaya terapiya i profilaktika, Prakticheskaya meditsina, Moscow, Russia (2012) [in Russian]. ISBN 978-5-98811-219-8.
2. A. M. Enejder, T. W. Koo, J. Oh, M. Hunter, S. Sasic, M. S. Feld, and G. L. Horowitz, "Blood analysis by Raman spectroscopy", Optics Letters 27(22), 2004-2006 (2002).
3. A. Rygula, K. Majzner, K. M. Marzec, A. Kaczor, M. Pilarczyk, and M. Baranska, "Raman spectroscopy of proteins: a review", Journal of Raman Spectroscopy 44(8), 1061-1076 (2013).
4. G. A. Zalesskaya, E. G. Sambor, "Interaction of low-intensity laser radiation with blood and its components", Journal of Applied Spectroscopy 72(2), 230-235 (2005) [in Russian].
5. A. N. Malov, A. Y. Seteikin, A. V. Neupokoeva, E. S. Musatova, I. E. Golub, L. V. Sorokina, V. S. Fetschenko, and A. A. Vaichas, "The laser radiation action on the biological objects", Optik 124(23), 6034-6041 (2013).
6. R. A. Paringer, A. V. Kupriyanov, and N. Y. Ilyasova, "Dendritic crystallogram images classification", Journal of Biomedical Photonics & Engineering 1(2), 135-138 (2015).
7. A. N. Malov, A. V. Neupokoeva, "A «chessboard» method for the speckle images analysis", Holography. Science and practice. Collection of works of the 10th International Conference "GoloExpo 2013", OOO «MNGS», Moscow, 257-264 (2013) [in Russian].
8. M. A. Vilensky, D. N. Agafonov, D. A. Zimnyakov, V. V. Tuchin, and R. A. Zdrazhevsky, "Speckle-correlation analysis of microcapillary blood flow in the nail bed," Quantum Electronics 41(4), 324–328 (2011).
9. S. V. Moskvin, Osnovy lazernoy terapii. Seriya "Effektivnaya lazernaya terapiya," Triada, Tver (2016) [in Russian].
10. A. N. Malov, A. V. Neupokoyeva, and L. A. Kokorina, "Laser modification of liquid nutrient medium and antibiotic solutions with the assessment by the bacteria growth dynamics," The Journal of Biomedical Photonics & Engineering 3(2), 020303 (2017).
11. Y. Y. Tarasevich, "The models and mechanisms of the dehydration self-organization of biological fluids," Physics-Uspekhi 47(7), 717-728 (2004).
12. E. G. Rapis, "A change in the physical state of a nonequilibrium blood plasma protein film in patients with carcinoma," Technical Physics 47(4), 510-512 (2002).

13. A. I. Andryushkin, S. P. Sapozhnikov, and A. V. Karpunina, “Crystallography of biological fluids (a review),” Vestnik Chuvashskogo Universiteta 3, 355-359 (2013) [in Russian].
14. P. V. Pavlov, A. N. Malov, A. V. Neupokoeva, and F. N. Popov, “A testing method for machine details state by means of the speckle image parameters analysis”, Proceedings of SPIE 10176, 101760Z (2016).

Influence of laser irradiation on the activity of plant pharmaceuticals with the assessment by the bacteria growth dynamics

Lubov A. Kokorina and Anna V. Neupokoeva*
Irkutsk State Medical University, 1 Krasnogo Vosstaniya Str., Irkutsk, 664009 Russia

*** e-mail:** annett_2005@inbox.ru

Abstract. The article describes experimental investigation of influence of laser irradiation on the drug activity of umbellate wintergreen and round-leaved wintergreen in the form of decoction and extract. The drug activity is estimated by counting the number of colonies grown on the nutrient medium with the addition of the studied plant preparation. It is shown that laser irradiation of pharmaceuticals significantly changes their activity, and the best results are obtained by irradiation of the umbellate wintergreen decoction. © 2019 Journal of Biomedical Photonics & Engineering.

Keywords: laser; drug activation.

Paper #3315 received 10 Feb 2019; revised manuscript received 17 Mar 2019; accepted for publication 3 Apr 2019; published online 13 May 2019. doi: 10.18287/JBPE19.05.020302.

1 Introduction

Modern trends of medical and biological laser radiation application can be divided into two main groups. The first group uses unique properties of laser radiation as a research tool: spectral analysis, laser microscopy, holography, etc. The second group uses laser radiation for influence on biological objects: in therapy, surgery and diagnosis.

At present, many researchers have shown in practice that complex using of laser radiation and standard drugs for the treatment of various human diseases is more effective than their separate using [1-7]. This approach is often due to the fact that modern antibiotics are not always effective, since most bacteria have learned to defend themselves. So some strains of Staphylococcus aureus acquired resistance to a wide range of antibiotics, in particular to penicillins (methicillin, dicloxacillin, nafcillin, oxacillin, etc.) and cephalosporins. This leads to various complications after staphylococcal infection and causes high mortality. Therefore, search for new drugs or modification of existing ones under influence of laser radiation is an important direction.

On the other hand, most drugs are used in the form of liquids: solutions, emulsions, extracts, etc. When large organic molecules (primarily proteins and polypeptides) dissolve in water, a solution like colloidal is formed. At the micro level, this means that protein macromolecules do not break down into simpler components but rather acquire a hydrate shell transferring part of the water molecules into a bound state. Thus, dissolved substances form clusters (associates) by combining molecules due to electrostatic interaction forces [8, 9]. A cluster can consist of several tens of molecules, which leads to decreasing their mobility and reactivity, because active centers can be overlapped by near-located molecules. Therefore, destruction of clusters into components would increase biochemical activity of molecules, and hence activity of the solution as a whole.

As a rule, the molecules in the cluster are bound by hydrogen or hydrophobic interactions, so such formations are unstable and must be destroyed by physical factors. Thus, it is known [10, 11] that under action of laser radiation clusters are able to decay into smaller formations, since coherent monochromatic laser radiation causes intensive movement of charged areas of macromolecules, as a result of which molecules break out of clusters, creating a homogeneous mixture with fewer inhomogeneities.

The aim of our work is assessing change in the plant drugs activity of umbellate wintergreen (*Chimaphila umbellate (L.) W. Barton*) and round-leaved wintergreen (*Pyrola Rotundifolia*) to *Staphylococcus aureus* under influence of laser radiation.

2 Experiment

2.1 Materials and methods

For experimental studies, we used reference strain Staphylococcus aureus – gram-positive, regular shape globular cells in the smear are arranged in clusters in the form of "grapes". They are included in the group of conditionally pathogenic microorganisms, which are sensitive to ampicillin. Temperature optimum for bacterial growth is 25–35 ºC, optimum pH is 7.0–7.5. Meat-peptone agar (MPA) was used to cultivate bacteria.

Impact on plant drugs before its adding to nutrient medium was carried out in the "light boiler" mode. The duration of exposure was 20 and 60 seconds. The radiation power was about 100 mW, the wavelength was 532 nm, and total irradiation energy was about 5 J/g.

The choice of plants as a drugs source was due to the fact that both the umbellate wintergreen and round-leaved wintergreen are widely used as antiseptics, anti-inflammatory and antimicrobial drugs. Their composition is well known, in particular, both plants contain flavonoids, tannins, triterpenoids. All these components can provide antimicrobial activity [12].

There were two types of umbellate wintergreen preparations: herbal decoction and alcohol tincture (extract) in experiments. The concentration of the active substance in the decoction was 0.025%, and in the extract – 0.06%. Also in experiments, two types of round-leaved wintergreen preparations were used: herbal decoction and alcohol tincture (extract). The concentration of the active substance in the decoction and in the extract was the same – 0.01%. These drugs were exposed by laser radiation for 20 and 60 seconds. Control (C) was a sterile physiological solution, positive control (C+) was ampicillin solution (penicillin semisynthetic) – broad-spectrum antibiotic at a concentration of 1 μg/ml.

In the *experiments by scheme 1* we studied the colonies grow dynamics on MPA. 1 ml of bacterial suspension and 1 ml of the test solution were added to the flask with the nutrient medium. The flask's contents were mixed and poured into Petri dishes, which then were placed in a thermostat (37–38 ºC). Colonies number counting was made every 12 hours.

In the *experiments by scheme 2,* we estimated influence of laser radiation on the drugs antibacterial activity by measuring of the growth inhibition zone [13]. 1 ml suspension of microorganisms was added to the flasks with 100 ml MPA, and then the resulting mixture was poured into Petri dishes. After agar gelation three holes of the same diameter were made in the MPA medium. Non-irradiated and irradiated drugs were added in the holes and then Petri dishes were put in thermostat under 37 ºC. After 12 hours we measured the diameter of growth inhibition zones with accuracy within 1 mm.

2.2 Results and discussion

During the experiments the colonies growth dynamics on the agar medium (MPA) was recorded by measuring the total number of grown colonies every 12 hours. Further, the obtained data were averaged over three series of experiments, the error did not exceed 11% (Fig. 1).

Data comparison (Fig. 1) shows that the irradiated umbellate wintergreen decoction inhibits the *St. aureus* colonies growth. The most pronounced effect was observed under the action of the drug irradiated for 60 seconds (the number of colonies is 12-14% of the control). Whereas, in the experiment with non-irradiated decoction colonies number was more than control (103% for 12 hours after the cultivation start).

Under the action of the not irradiated extract the grown colonies number was 64% of the control by the end of the observations. It represents a weak bactericidal effect compared to the irradiated drug for that the number of bacterial colonies was 33% and 42% of the control for time exposure 20 seconds and 60 seconds respectively. Thus, irradiated umbellate wintergreen extract inhibits the bacteria growth stronger than not irradiated, and the laser exposure duration doesn't play a significant role, because the difference is comparable to the measurement error. Ampicillin inhibits the growth of *St. aureus* completely.

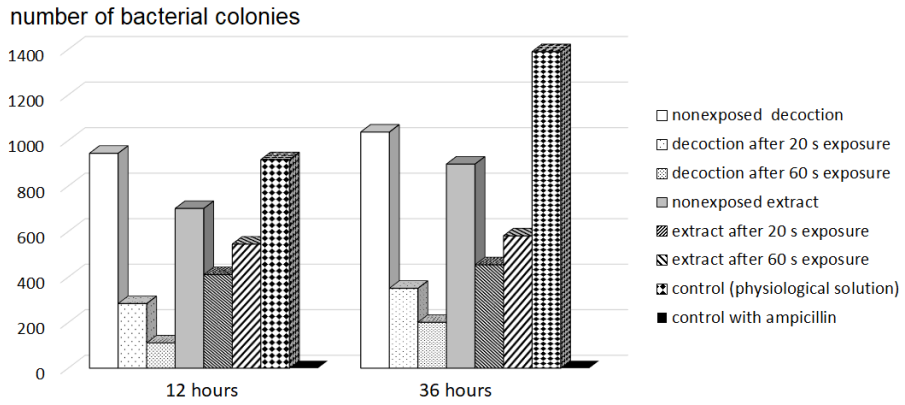

Fig. 1 Colonies growth dynamics on agar medium with the addition of decoction and extract of umbellate wintergreen.

Photos of grown colonies on MPA in the analyzed experiments are presented in Fig. 2. Experiments was carried out by the diffusion in agar method. Drugs antimicrobial activity was recorded by size measurement of Staphylococcus growth inhibition zone [13], which was formed after 12 hours of cultivation.

Growth inhibition zones were not found in experiments with non-irradiated umbellate wintergreen decoction, as well as in the control version. Laser irradiation of the decoction led to the bactericidal activity appearance: the growth inhibition zones were 12 and 13 mm and bactericidal activity did not significant depend on exposure time. Ampicillin (K+) actively suppresses the *Staphylococcus aureus* growth, the suppression zone size was from 23 to 30 mm. Ampicillin bactericidal activity was not changed under laser exposure for 20 and 60 seconds.

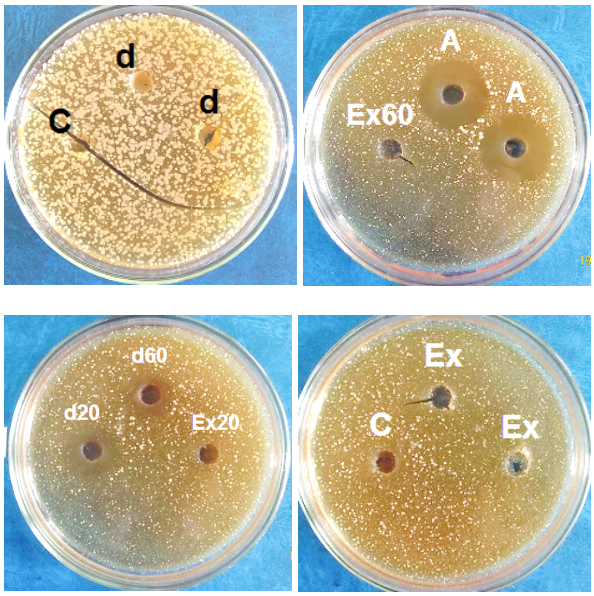

Fig. 2 Growth inhibition zone of the experiments with umbellate wintergreen drugs: C – control (physiological solution), d – non exposed wintergreen decoction, d20 – wintergreen decoction after 20 second exposure, d60 – wintergreen decoction after 60 second exposure, Ex – non exposed wintergreen extract, Ex20 – wintergreen extract after 20 second exposure, Ex60 – wintergreen extract after 60 second exposure, A – control with ampicillin.

Experimental data for round-leaved wintergreen are shown in Fig. 3, the error does not exceed 26%. According to the diagram (Fig. 3) on the first day the bactericidal effect is expressed in the non-irradiated and irradiated round-leaved wintergreen decoction, as well as in the non-irradiated round-leaved wintergreen extract: the number of colonies is 60–80% of the control. At the same time, irradiated extract stimulate the *St. aureus* growth (133% compared to control). After 48 hours from the start of observation round-leaved wintergreen decoction, both irradiated and non-irradiated, retain bactericidal activity. And, preparations based on the extract do not have any stimulating or bactericidal effect, i.e. do not cause significant changes in the bacteria growth compared to the control.

Ampicillin completely inhibits the growth of bacteria.

Bactericidal activity registration by diffusion in agar method was carried out 12 hours after the cultivation start. The experiment showed that non-irradiated and irradiated preparations of round-leaved wintergreen do not lead to the appearance of growth inhibition zones.

3 Conclusions

Bactericidal activity of plant preparations on the base of umbellate wintergreen and round-leaved wintergreen in two dosage forms (decoction and alcohol extract), irradiated with low-intensity laser radiation was investigated. The minimum colonies growth was observed under the action of 20 and 60 seconds irradiated umbellate wintergreen preparations (decoction and alcohol extract). It was also found that the non-irradiated umbellate wintergreen decoction did not lead to the suppression of *St. aureus* growth, but laser irradiation of the drug causes bactericidal activity appearance, which is significantly different from the control. Non-irradiated extract leads to weak inhibition of *St. aureus* growth, but the irradiated drug bactericidal activity increases almost 2 times in comparing with non-irradiated, regardless of the laser exposure time.

Bactericidal action of umbellate wintergreen decoction was not revealed by the diffusion in agar method, while the irradiated drug caused the growth inhibition zones appearance. Under the diffusion in the culture medium of non-irradiated umbellate wintergreen extract and irradiated preparations bactericidal action is not revealed.

A moderate bactericidal effect was found under applying a round-leaved wintergreen decoction, but statistically significant differences caused by laser irradiation of the drug compared with the control was not detected.

It is necessary to note that the bactericidal activity of drugs is due to the whole complex of components of the plant raw materials. Without special studies it is impossible to separate a single component that suppresses the bacteria growth. According to the literature data [12], bactericidal activity can be provided by flavonoids and triterpenoids, and the inhibition mechanisms of bacterial growth can be different: direct membranes destruction, binding to protein complexes, which violates the specific function of the protein, violation of enzyme – substrate interaction by binding to one of them. In all these cases, the drug activity is affected by the number of molecules that can interact with the membrane or proteins, as well as their aqueous environment. The combination of several molecules to a cluster surrounded by a hydrate shell reduces their activity.

Decoction-based preparations contain about 80% water and do not contain ethanol. Preparations based on the extract contain only 56% water and 38% alcohol (ethanol). Therefore, in alcohol extracts, the

antibacterial activity of molecules can be reduced by interacting with ethanol, which not only changes the oxidative activity of organic molecules, but also transforms some water into a bound state.

A significant difference in the bactericidal action of the umbellate wintergreen and round-leaved wintergreen drugs due to different chemical composition and ratio of components. However, the phenomenon of bacterial growth stimulation by irradiated round-leaved wintergreen extract, despite the fact that the non-irradiated extract, on the contrary, has a bactericidal effect, requires further research.

Disclosures

All authors declare that there is no conflict of interests in this paper.

References

1. A. V. Nikitin, M. F. Gorbatykh, E. F. Evstratova, and S. A. Fisunova, "Changes in pro-inflammatory cytokines and oxidative status in patients with psoriatic arthritis during treatment with a combination of arthrofoon with low-intensity laser radiation," Bulletin of new medical technologies 19(2), 260–263 (2012) [In Russian].
2. Y. N. Chernykh, V. A. Valuyev, "Evaluation of the effectiveness of low-intensity laser radiation in the complex treatment of patients with chronic obstructive pulmonary disease," Bulletin of new medical technologies 18(2), 323–325 (2011) [In Russian].
3. A. V. Lebedeva, D. A. Malyukov, and A. V. Nikitin, "Low-intensity laser radiation and immunofuran in the complex therapy of chronic obstructive pulmonary disease," Bulletin of new medical technologies17(2), 214–216 (2010) [In Russian].
4. G. V. Maksimov, A. V. Nagovitsyn, "The role of low molecular weight proteins in the implementation of the action of laser radiation and an alternating magnetic field on the blood," Bulletin of Moscow University. Series 16: Biology 3, 8–12 (2009) [In Russian].
5. G. A. Zalesskaya, E.G. Sambor, "Interaction of low-intensity laser radiation with blood and its components," Journal of Applied Spectroscopy 72(2), 230–235 (2005).
6. V. F. Kirichuk, O. V. Khlebina, "The nature of changes in endogenous intoxication, lipid peroxidation in patients with inflammatory processes of the uterus appendages in combination with standard treatment with helium-neon laser radiation," Basic research 11, 69–73 (2010) [In Russian].
7. A. P. Manzhos, Optimization of the use of low-intensity infrared laser radiation in the treatment of bronchial obstruction with a stable course of chronic obstructive pulmonary disease, PhD thesis, Moscow (2007) [In Russian].
8. A. V. Finkelshtein, O.B. Ptitsyn, Protein Physics, Knizhyi dom "Universitet", Moscow, Russia (2002) [in Russian].
9. V. D. Lakhno, Clusters in Physics, Chemistry, Biology, NITs "Regular and chaotic dynamics", Izhevsk, Russia (2001) [in Russian].
10. A. N. Malov, A. A. Vaichas, Laser Control of Biomineral Formation. Physical Principles and Prospects of Developing New Medical Nanotechnology, Palmarium Academic Publishing, Saarbrucken, Deutschland (2016) (ISBN 978-3-659-60476-8) [in Russian].
11. A. N. Malov, A. Y. Seteikin, A. V. Neupokoeva, E. S. Musatova, I. E. Golub, L. V. Sorokina, V. S. Fetschenko, and A. A. Vaichas, "The laser radiation action on the biological objects," Optik 124(23), 6034–6041 (2013).
12. M. M. Cowan, "Plant Products as Antimicrobial Agents," Clinical Microbiology Reviews 12(4), 564–582 (1999).
13. Determination of antimicrobial activity of antibiotics using the method of diffusion into agar. State Quality Standard of Medical Agent. General Pharmacopeia Article, Ministry of Health of Russian Federation (2010) [in Russian].

IR spectra of porous silicon based nanocomposites

Kristina A. Ganichkina*, Diana R. Suyundukova, and Natalya V. Latukhina
Samara National Research University, 34 Moskovskoe shosse, Samara 443086, Russian Federation

*** e-mail:** ganichkina.k@mail.ru

Abstract. The article is devoted to the problem of using porous silicon (por-Si) as a biomaterial. IR spectroscopy was used to study the composition of por-Si samples and nanocomposites: por-Si with hydroxyapatite, promising as a biomaterial for osteoplasty and por-Si with glucose (for biosensor). The studies were carried out on the FSM 2201 Fourier spectrometer using the diffuse reflection prefix and Perkin Elmer Spectrum 100 using the total internal reflection violation prefix. A comparative analysis of the results shows a noticeable difference between the IR spectra of nanocomposites and the IR spectrum of the original por-Si and allows to identify the substance in the pores. © 2019 Journal of Biomedical Photonics & Engineering.

Keywords: glucose; hydroxyapatite; nanocomposite; biosensor; IR spectroscopy.

Paper #3313 received 30 Jan 2019; revised manuscript received 3 Apr 2019; accepted for publication 1 May 2019; published online 27 May 2019. doi: 10.18287/JBPE19.05.020303.

1 Introduction

The future of medicine is to increase the accuracy of diagnosis and dosage of drugs, working out of medicinal agent with a new principle of effect, which should lead to an increase in the duration of a full human life. Nanomaterials and nanotechnologies play an indispensable role in solving these problems. Biosensors based on nanomaterials open up wide possibilities of obtaining information much faster, easier and more accurate than it happens with the help of traditional analysis. The role of nanotechnology is also important in the creation of bone and other implants, where nanoporous and nanocomposite materials show better survival in the body.

Por-Si with a developed pore system and, as a consequence, a large area of the inner surface, is promising for various medical applications, as well as other porous nanomaterials. An additional advantage is its biocompatibility, while the por-Si can be both bio-resistant and bio-resorbable, and its dissolution products are non-toxic [1, 2]. Promising areas of por-Si application in medicine may include the creation of a microchip of the artificial retina [3], the destruction of cancer cells using por-Si nanoparticles [4, 5], the cultivation of biological tissues on the por-Si surface [6, 7], the creation of nanostructured containers for drug delivery [8, 9], ultra-sensitive biosensors [10, 11], and much more. The presence of a large number of pores allows the use of por-Si to create a variety of nanocomposites, which further expands the scope of its possible applications.

The purpose of our work is to determine the possibility of using the por-Si for the blood glucose biosensor, and the possibility of creating biomaterials for osteoplasty based on nanocomposites of silica with hydroxyapatite (HAP) – mineral phase of bone. For this purpose, the IR spectra of material samples based on por-Si nanocomposites with glucose and HAP were studied. Analysis of IR spectra allows determining the phase composition of the material, the presence of the necessary substances and the absence of undesirable ones.

2 Porous silicon as a biomaterial for medicine

2.1 Bone implants based on hydroxyapatite and silicon

Developed chemically active surface and high adsorption capacity in relation to biological and organic molecules determines the possibility of using por-Si as a substrate for tissue growth. The possibility of growth on the surface of por-Si of a wide variety of biological tissues, from skin and bone to brain tissue, has been experimentally shown [6, 7]. The advantages of using por-Si in polymer-based materials for osteoplasty are

also shown [12, 13]. Por-Si based biodegradable material, which applied to the fracture area, will ensure rapid recovery of the damaged bone without the use of any pins or tires and over time will be completely replaced by the patient's own bone tissue [13].

At the initial stage, silicon plays a significant role in the formation of bone, accelerates the process of calcification, which contributes to faster and stronger bone formation. Silicon ions in combination with hydroxyapatite fill the "skeleton" of the bone at the molecular level and make the skeleton tissue more dense [13].

HAP saturated por-Si can serve as a basis for the creation of transport particles for the delivery of hydroxyapatite to the affected areas of the bone in case of any injuries or diseases, for example, osteoporosis [14, 15]. There is important that during the saturation of the HAP pores absence of chemical interaction of substances with the formation of undesirable insoluble compounds such as silicates or silicides, is need, because such interaction will worsen the dissolution of transport particles and reduce the proportion of useful "building material". In this regard, the study of IR spectra of nanocomposite por-Si + HAP is very important.

2.2 Prospects of creating a biosensor based on porous silicon

Por-Si is a promising platform for the creation of biosensors. The diversity of the pore structure leads to a variety of optical, electrical and mechanical characteristics of the material. An important feature of porous silicon is its high adsorption capacity to biological and organic molecules. Adsorption affects electronic properties, the change of which leads to changes in the type and nature of surface active centers. This property of silicon is used in medicine to create materials for biosensors [16, 17].

The first glucose-determining biosensor, ExacTech (MediSense), used an electrode containing glucose oxidase as an enzyme [18]. However, it is possible to create a biosensor based on a por-Si without the use of enzymes, because the modification of the surface of the por-Si leads to different values of the sensitivity to glucose and the correct choice of the parameters of the layers it is possible to obtain the maximum value of sensitivity.

The optical properties of porous silicon are the promise for creating biosensors. Optical methods of blood glucose determination are the most attractive because they are safe for humans [18–20]. One of the promising optical methods is the method of analysis of IR spectra of human physiological fluids – blood, plasma, saliva, tears [20]. Therefore, in this work, the study of IR spectra of por-Si composites with aqueous glucose solutions was carried out.

3 Methods of creation and investigation of nanocomposites from your por-Si

3.1 Creation of nanocomposite samples

The method of horizontal electrochemical etching (Fig. 1) was used to obtain por-Si samples. Silicon wafers with three different types of surfaces: faceted, textured and polished were used. Initially, the silicon plates are cleaned of organic contaminants, they are boiled for 5 minutes in a solution of hydrogen peroxide (H_2O_2), ammonia hydrate (NH_4OH) and water (H_2O), mixed in a ratio of 1:1:4 and dried at room temperature.

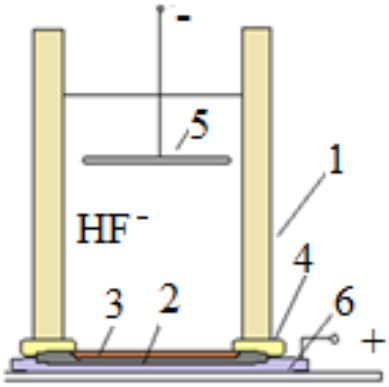

Fig. 1 The scheme of the electrolytic cell for the formation of layers of porous silicon (1 – fluoroplastic bath, 2 – silicon wafer, 3 – layer of porous silicon, 4 – seals, 5 – platinum electrode, 6 – metal electrode).

After that, the plate is placed in an electrolytic cell. A silicon plate is placed on the metal electrode, a fluoroplastic bath is installed on it, which is then filled with electrolyte, the platinum electrode is immersed in the electrolyte. In the process, electrolytes based on aqueous-alcoholic solutions of hydrofluoric acid with the addition of ammonium fluoride were used. Etching lasted 20, 25 and 30 minutes at a voltage U = 30 V and a current I = 40 mA. Etching under these conditions is quite equal, building up a system of vertical parallel pores ten micrometers deep. The pore depth depends on the etching time and anode current density.

To create a glucose nanocomposite the solutions of glucose powders ($C_6H_{12}O_6$) in water with different concentration were used. Por-Si nanocomposite with HAP was created by hap deposition on a substrate from a suspension in ethyl alcohol (10 ml – alcohol: 170.8 mg – HAP). The deposition time was 30 minutes, after which the excess suspension from the por-Si surface was removed.

3.2 The IR-spectroscopy method

IR spectra were recorded by the Fourier spectrometer Perkin Elmer Spectrum100 with the prefix of disturbed total internal reflection (FTIR). Also, for comparison, IR spectra were taken by the FSM 2201 with the diffuse reflection prefix.

4 Analysis of results

The Figs. bellow show the comparative IR spectra measured on the FSM-2201 spectrometer for glucose, the control sample of the plate, samples with 6% and 12% glucose solutions on the por-Si (Fig. 2). In the Figs., the red color indicates the control samples with the rough ground (indicated by the letter N) and polished (indicated by the letter X) surface, blue samples with 6% glucose solution, green samples with 12% glucose solution, and pink spectrum of glucose powder.

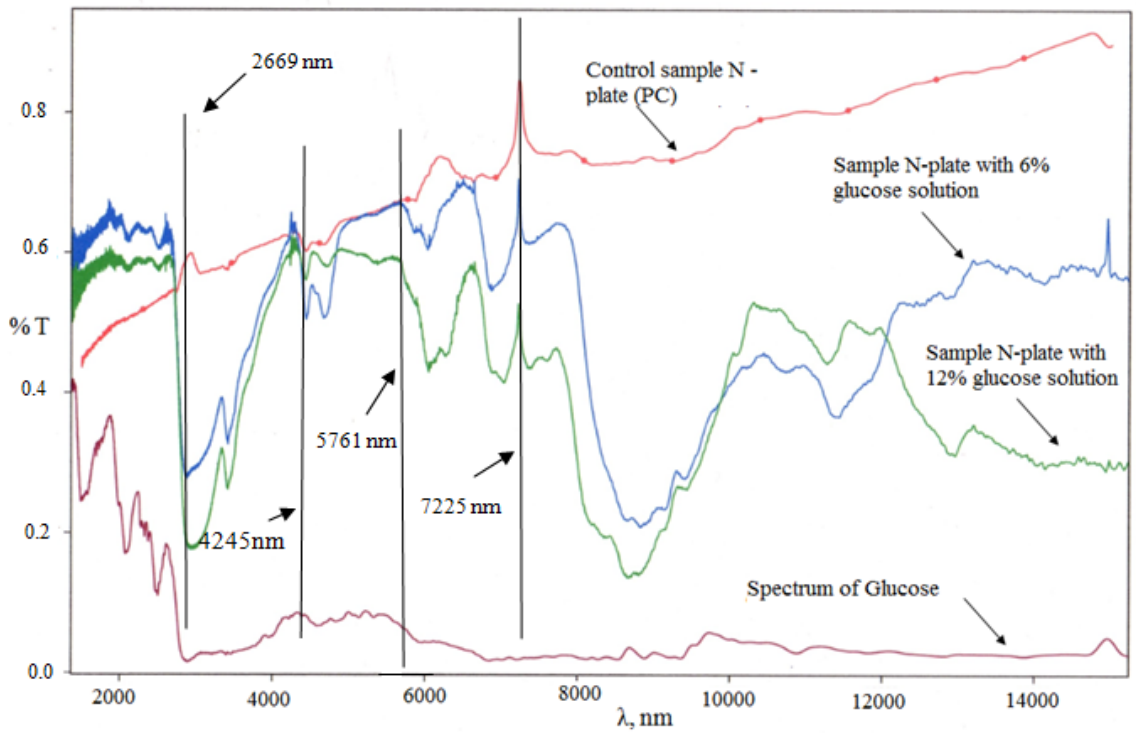

(a)

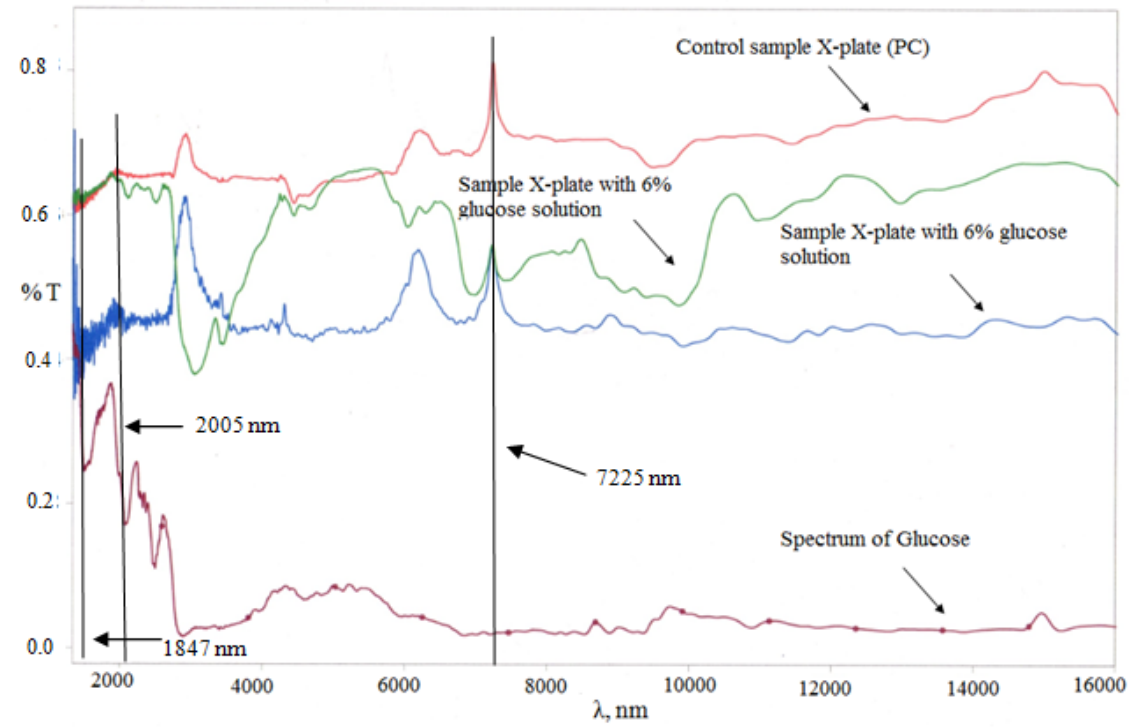

(b)

Fig. 2 (a) IR spectra for N-plate with rough ground surface; (b) IR spectra for X-plate with polished surface.

The figures demonstrate that the saturation of the pores with an aqueous solution of glucose significantly changes the appearance of the IR spectrum (red lines in comparison with blue and green); this is especially noticeable for samples with a polished surface. Spectra of the nanocomposite samples of por-Si with glucose are impossible to obtain as a simple superposition of the spectra of the original por-Si and powder glucose. Certain absorption bands are responsible for silicon, and some bands for the presence of glucose in the pores of the samples. Absorption bands of porous silicon are clearly visible: peak 7225 nm, 4245 nm, 5761 nm. The bands responsible for the presence of glucose can be observed at 1847 nm, 2005 nm, 2669 nm. These bands can identify the presence of glucose in the liquid. However, for samples with different surface treatment, both the height and position of the glucose peaks are different. Therefore, for the quantitative analysis of the glucose content in the nanocomposite, some unification of the surface of the samples is necessary.

The analysis by IR spectroscopy was carried out for samples of nanocomposite por-Si + HAP on the spectrometer "Perkin Elmer Spectrum 100". The spectra of the initial silicon wafer, a plate with a porous layer, a porous layer saturated with HAP and a powder of por-Si nanocomposite with HAP were measured. Identification of absorption bands was carried out according to the tables of characteristic frequencies on the basis of literature and reference data [20, 21].

The additional absorption bands appear in the IR spectrum of the por-Si (Fig. 3(2)) in comparison with silicon. The por-Si surface is covered by SiH_2 groups. This is evidenced by the presence of the absorption band 624 cm^{-1} corresponding to the deformation vibrations. In order to determine whether hydroxyapatite is contained in the pores, the IR spectrum of hydroxyapatite itself is given (Fig. 3(3)). The identification method revealed that the absorption peaks in both samples correspond to each other, which indicates the HAP content in the pores of silicon. The presence of HAP in the porous layer significantly changes the appearance of the IR spectra of the samples (Fig. 3(4)). IR spectrum of por-Si + HAP powder is shown in figure 3/5 (Fig. 3(5)). Absorption peaks at 1062 cm^{-1}, 977 cm^{-1}, 874 cm^{-1}, 604 cm^{-1}, clearly expressed in the HAP spectrum, are present in the spectra of both nanocomposite and nanocomposite powder. At the same time, no additional peaks appear in the spectra. Hence, we can conclude that some new compounds in the saturation of the pores HAP is not formed, that is, the chemical interaction of por-Si and HAP is absent.

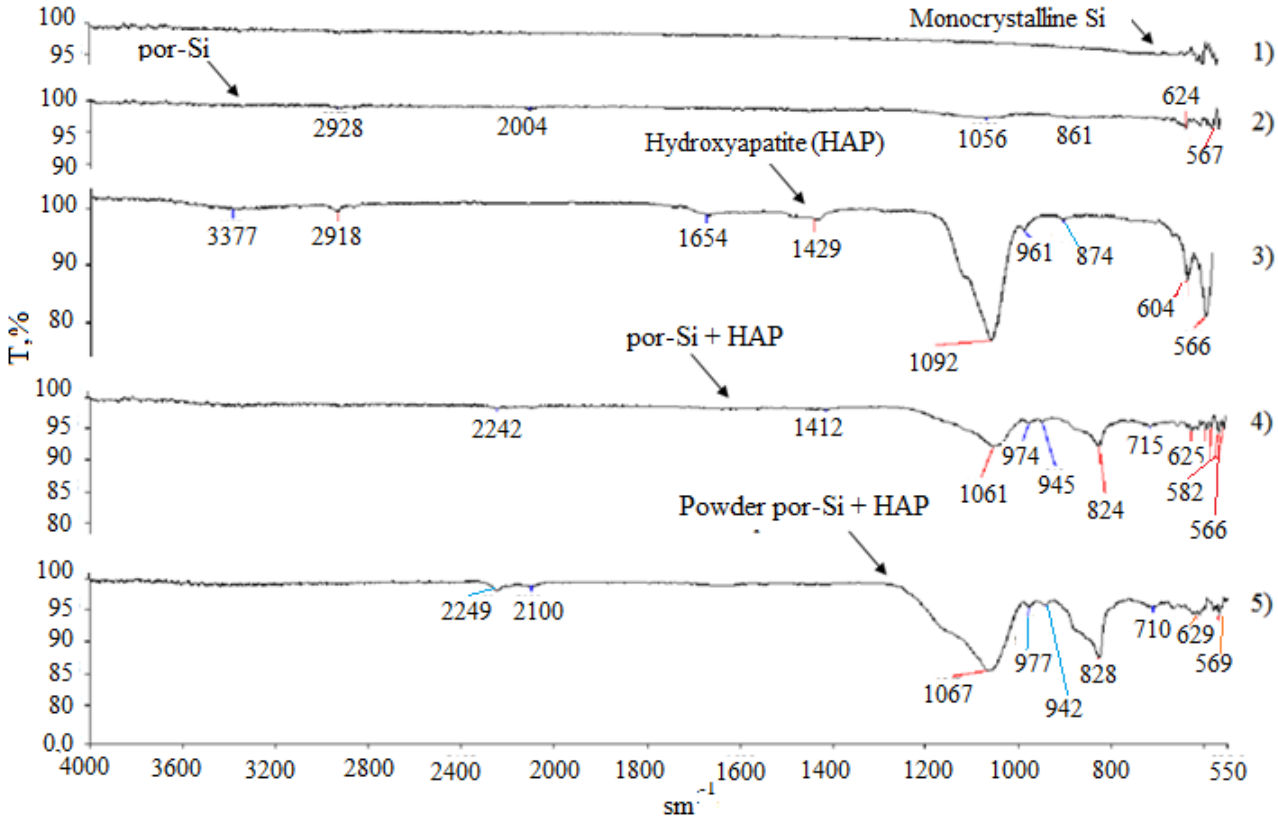

Fig. 3 IR spectra 1) monocrystalline Si, 2) por-Si, 3) hydroxyapatite, 4) por-Si + HAP, 5) por-Si + HAP Powder obtained on the FSM spectrometer Perkin Elmer Spectrum100.

5 Conclusions

The results of the analysis of the work may be concluded as bellow.

1. IR spectroscopy study of por-Si + glucose nanocomposites approve that the presence of glucose in the pores significantly changes the transmission spectra of the samples: the spectra show new bandwidth at 1847 nm, 2005 nm, 2669 nm. For the development of a por-Si-based material suitable for use in a glucose biosensor, it is necessary to provide for the unification of the surface of the samples.

2. IR spectroscopy revealed that there is no chemical interaction between the substances of hydroxyapatite and porous silicon. On the IR spectra of all por-Si samples with HAP there are only peaks corresponding to the bonds in the por-Si or HAP.

It may be concluded that porous silicon is a promising material for the creation of glucose biosensor and the nanocomposite systems por-Si + HAP are suitable for the manufacture of biomaterial for bone implants and drugs for the treatment of osteoporosis.

Disclosures

All authors declare that there is no conflict of interests in this paper.

References

1. M. Simion, I. Kleps, T. Neghina, A. Angelescu, M. Miu, A. Bragaru, M. Danila, E. Condac, M. Costache, and L. Savu, "Nanoporous silicon matrix used as biomaterial," Journal of Alloys and Compounds 434–435, 830–832 (2007).
2. O. I. Ksenofontova, A. V. Vasin, V. V. Egorov, , A. V. Bobyl', F. Y. Soldatenkov, E. I. Terukov, V. P. Ulin, N. V. Ulin, and O. I. Kiselev, "Porous silicon and its applications in biology and medicine," Technical Physics59(1), 66–77 (2014).
3. N. V. Latuhina, G. A. Pisarenko, A. V. Volkov, and V. A. Kitaeva, "Fotochuvstvitel'naya matrica na osnove poristogo mikrokristallicheskogo kremniya," Vestnik Samarskogo gos. universiteta. Estestvennonauchnaya seriya 5(86), 115–121 (2011) [in Russian].
4. C. Lee, H. Kim, C. Hong, M. Kim, S. S. Hong, D. H. Lee, and W. I. Lee, "Porous silicon as an agent for cancer thermotherapy based on near-infrared light irradiation," Journal of Materials Chemistry 18(40), 4790–4795 (2008).
5. L. A. Osminkina, K. P. Tamarov, A. P. Sviridov, R. A. Galkin, M. B. Gongalsky, V. V. Solovyev, A. A. Kudryavtsev, and V. Y. Timoshenko, "Photoluminescent biocompatible silicon nanoparticles for cancer theranostic applications," Journal of Biophotonics 5(7), 529–535 (2012).
6. L. Pramatarova, E. Pecheva, D. Dimova-Malinovska, R. Pramatarova, U. Bismayerc, T. Petrov, and N. Minkovski, "Porous silicon as a substrate for hydroxyapatite growth," Vacuum 76(2–3), 135–138 (2004).
7. J. L. Coffer, M. A. Whitehead, D. K. Nagesha, P. Mukherjee, G. Akkaraju, M. Totolici, R. S. Saffie, and L. T. Canham, "Porous silicon-based scaffolds for tissue engineering and other biomedical applications," Physica Status Solidi (A) 202(8), 1451–1455 (2005).
8. T. J. Barnes, L. J. Karyn, and C. A. Prestidge, "Recent advances in porous silicon technology for drug delivery," Therapeutic Delivery 4(7), 811–823 (2013).
9. Y. M. Spivak, N. R. Nigmadzyanova, "Poluchenie poristogo kremhiya dlya primeneniya v adresnoy dostavke lekarctv," Molodoy ucheniy 10, 208–212 (2014) [in Russian].
10. S. Dhanekar, S. Jain, "Porous silicon biosensor: Current status," Biosensors and Bioelectronics 41, 54–64 (2013).
11. B. Gupta, Y. Zhu, B. Guan, P. J. Reece, and J. Gooding, "Functionalised porous silicon as a biosensor: emphasis on monitoring cells in vivo and in vitro," The Analyst 138(13), 3593–3615 (2013).
12. D. Fan, G. R. Akkaraju, E. F. Couch, L. T. Canham, and J. L. Coffer, "The role of nanostructured mesoporous silicon in discriminating in vitro calcification for electrospun composite tissue engineering scaffolds," Nanoscale 3(2), 354–61 (2011).
13. M. A. Whitehead, D. Fan, G. R. Akkaraju, L. T. Canham, and J. L. Coffer, "Accelerated calcification in electrically conductive polymer composites comprised of poly(epsilon-caprolactone), polyaniline, and bioactive mesoporous silicon," Journal of Biomedical Materials Research Part A 83A(1), 225–234 (2007).
14. E. M. Carlisle, "Silicon as a trace nutrient," Science of The Total Environment 73(1–2), 95–106 (1988).
15. E. V. Berlova, A. S. Domchenkova, V. A. Zhukova, and N. V. Latuhin, "Nanokomposity poristogo kremniya s gidroksiapapitom dlyamedicinskih prilozheniy," Sbornic materialov V Vserossiyskoy konferencii po nanomaterialam "Nano 2013", 382 (2013) [in Russian].
16. S. Zairi, C. Martelet, N. Jaffrezic-Renault, R. M'gaïeth, H. Maâref, and R. Lamartine, "Porous silicon a transducer material for a high-sensitive (bio)chemical sensor: effect of a porosity, pores morphologies and a large surface area on a sensitivity," Thin Solid Films 383(1–2), 325–327 (2001).
17. Y. A. Vashpanov, I. P. Konup, V. A. Smyntyna, and V. A. Ivanica, "Vliyanie adsorbcii biologicheskih molecul na elektronnye parametry poristogo kremniya," Vestnic Odeskogo nacional'nogo Universiteta 11(7), 39–46 (2006) [in Russian].

18. N. Y. Arbatskaya, "Sovremennye pribory dlya samokontrolya urovnya sahara krovi," Lechashchiy vrach 5, 46–53 (2005).
19. "Nanotehnologii v medicine. Realnost ili poka tolko mif?" Nano News Net [in Russian].
20. N. A. Bazaev, Y. P. Masloboev, and S. V. Seliszhev, "Opticheskie metody neinvazivnogo opredeleniya urovnya glukozy v krovi," Medicinskaya tehnika 6(270), 29–33 (2011).
21. A. L. Smeth, Applied IR spectroscopy. Fundamentals, techniques and analytical problem solving, Wiley, New York (1979).
22. L. A. Kazicyna, N. B. Kupletskaya, Primenenie UF-, IK- I YaMR-spectroscopii v organicheskoy himii, Vysshaya shkola, Moscow (1971) [in Russian].

Optical methods of silicon nanoparticle diagnostics for applications in biomedicine

Alida F. Alykova[1*], Valery G. Yakunin[2], Victor Yu. Timoshenko[1,2,3], and Irina N. Zavestovskaya[1,3]

[1] National Research Nuclear University MEPhI (Moscow Engineering Physics Institute), 31 Kashirskoe shosse, Moscow 115409, Russian Federation

[2] Lomonosov Moscow State University, GSP-1 Leninskie Gory, Moscow 119991, Russian Federation

[3] P. N. Lebedev Physical Institute of the Russian Academy of Sciences, 53 Leninskiy Prospekt, Moscow 199991, Russian Federation

***e-mail:** AFAlykova@mephi.ru

Abstract. The method of Raman scattering spectroscopy was used to study various silicon nanostructures (nanowires, mesoporous nanoparticles, crystalline and laser-ablated nanoparticles) dispersed in aqueous medium. The obtained results indicate different dissolution rate for silicon nanoparticles of different sizes and morphology in water that can be used for their potential biomedical applications. © 2019 Journal of Biomedical Photonics & Engineering.

Keywords: silicon nanocrystals; nanowires; porous silicon; nanocrystalline silicon; laser ablated nanoparticles; Raman scattering; biodegradation.

Paper #3325 received 24 Apr 2019; revised manuscript received 4 Jun 2019; accepted for publication 4 Jun 2019; published online 29 Jun 2019. doi: 10.18287/JBPE19.05.020304.

1 Introduction

In recent years, various types of nanostructured forms of crystalline silicon (Si) have been intensively studied for application in technology and biomedicine, including for the diagnosis and therapy of various diseases [1, 2]. Porous Si [3, 4–7], silicon nanowires [8], and nanoparticles (NPs) obtained from them [9], as well as laser-ablated Si NPs [2, 10] and nanoparticles obtained from porous c-Si [11], have a great potential of unique physical and chemical properties for application both in tumor therapy [1, 2, 4, 9] and as contrast agents for bioimaging [8, 10, 11].

At present, several methods for obtaining powders and stable aqueous suspensions of Si NPs are known [1–6, 9, 10]. Photoluminescence (PL) of laser-ablated Si NPs, which is explained by radiative recombination of excitons excited in silicon nanocrystals with dimensions of 3–5 nm, was successfully applied in the study of the NP penetration into living cells [10]. It was found that Si NPs can be effectively accumulated in cancer cells and therefore they be used for diagnostics and therapy of cancer [2]. It was shown that the processes of accumulation and excretion of Si NPs in biological systems can be evaluated by the Raman spectroscopy [9].

In our work, we use the Raman scattering spectroscopy to study an effect of water exposure on the structural properties of crystalline Si nanowires (SiNWs), mesoporous silicon (meso-PSi), silicon nanocrystals (nc-Si) obtained by plasma-chemical synthesis or by the method of femtosecond laser ablation of c-Si targets in water (abl-Si).

2 Experimental technique

Samples of SiNWs were formed by metal-stimulated chemical etching (MSCE) of single-crystal silicon wafers (c-Si) of p-type conductivity with resistivity of 1–10 Om×cm and surface orientation (100) by using the standard two step approach (see e.g. Ref. [8]).

Meso-PSi samples were formed using the standard method of electrochemical etching plates c-Si p-type conductivity with surface orientation (100) and resistivity of 1–5 mOm×cm mixture of hydrofluoric acid and ethanol (HF(50%): C_2H_5OH=1:1) at a current density 60 mA/cm^2 for 1 hour.

After that, meso-PSi films were separated from the silicon substrate by a short-term increase in the current density up to 600 mA/cm^2. Aqueous suspensions of nanoparticles were obtained as a result of mechanical grinding of meso-PSi films in the planetary ball mill FRITSCH “Pulverisette 7” for 9 minutes at a rotation speed of 800 rpm and a diameter of 5 mm zirconium oxide balls used (see, for example, review [3]). Powders of nc-Si were obtained by the method of plasma-

chemical synthesis with the use of pure (99.9%) microcrystalline Si as the feedstock (see, for example, Ref. [1]).

The samples of SiNWs were placed in a 4 cm^3 cuvette filled with deionized water or saline (0.9% NaCl in H_2O) and held for a number of days. As a starting material, a sample with lateral sample sizes of about 1×1 cm and a nanowire length of about 10 μm was used. To study the dissolution of PF, aqueous suspensions of meso-PSi, nc-Si and abl-Si with a concentration of about 1 g/l in a volume of 10 ml were placed in dialysis bags with pore sizes of 6–10 kDa and kept from 1 to 24 hours in a large volume (5 liters) of deionized water at room temperature. Then at intervals 1, 2, 3, 6, 12, 24 hours some part of the suspension was collected, were planted on the stainless steel substrate, air-dried for 10–15 min and then examined by using the Raman scattering. All experiments were conducted at room temperature.

The Raman spectra of the obtained samples were taken on the DFS-52 spectrometer, which is located in the laboratory of the Department of low temperatures and superconductivity of MSU, in 90-degree scattering geometry. The receiver served working in the photon counting mode a cooled photomultiplier tube PMT-79. As a source of exciting radiation, an argon laser with wavelengths of 488 and 514.5 nm and a maximum intensity of not more than 100 W/cm^2 was used. The HORIBA Jobin Yvon LabRAM HR Visible micro-Raman spectrometer was used to measure Raman scattering spectra with excitation at a wavelength of 632.8 nm. The Raman spectra were also measured at the "Horiba Jobin Yvon" MicroRaman LabRAM HR Visible facility when excited by HeNe laser radiation with a wavelength of 632.8 nm or an argon laser with a wavelength of 488 nm. The signal was recorded in the backscattering geometry at normal incidence at room temperature in the air.

3 Results and discussion

Raman spectra of silicon nanowires with average cross-sectional dimensions of 20–100 nm before and after exposure to water or normal saline for 2 weeks are shown in Fig. 1. In the spectrum, there is a line at 520.5 cm^{-1} with width about 4 cm^{-1}, corresponding to the scattering on optical phonons of the c-Si crystal lattice. The high intensity of the line in comparison with single crystals of c-Si indicates the penetration of exciting radiation into the SiNWs layer followed by multiple scattering. The forms of the Raman scattering line in both c-Si and SiNWs samples are well described by the Lorentz function:

$$I_c(\omega) = \frac{C}{(\omega - \omega_c)^2 + \left(\frac{1}{2}\Delta\omega_c\right)^2}, \qquad (1)$$

where $\omega_c = 520.5$ cm^{-1} is the Raman phonon frequency in c-Si s, $\Delta\omega_c = 3$ cm^{-1} is the width of Raman line of c-Si at room temperature, C is a constant.

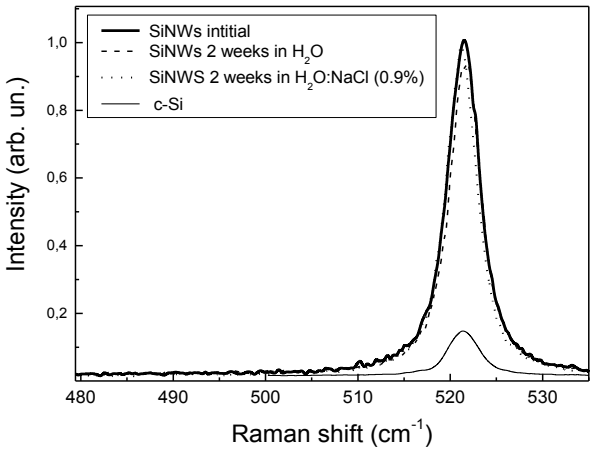

Fig. 1 Raman spectra of SiNWs before (thick solid line) and after storage in water (dotted line) and saline (punch line) for 2 weeks, as well as, for comparison, for c-Si substrate (thin solid line).

Obviously that the silicon nanowires in water and physiological (normal) saline solution do not exhibit a significant change of signal of Raman scattering which indicates the stability of the nanowires to dissolution. This stability is explained by the significant size of the cross section, as well as a sufficiently high quality oxide coating that occurs at the final stage of production.

When the samples are in water for one day meso-PSi silicon nanoparticles with the size of nanocrystals of about 10 nm demonstrate a multiple decrease in the intensity of Raman scattering, a shift in the band and an increase in the contribution of the amorphous phase of silicon, which indicates an effective dissolution (Fig. 2).

In accordance with Raman spectroscopy for meso-PSi we use the model proposed in Ref. [13]. According to this model limitations of the phonons to the nc-Si, we can use the following equation to form the line of Raman scattering [12, 13]:

$$I_{NC}(\omega) = \int_0^1 \frac{B\exp\left(-\frac{1}{4}q^2L^2\right)q^2}{(\omega - \omega_c(q))^2 + \left(\frac{1}{2}\Delta\omega_c\right)^2} dq, \qquad (2)$$

where $\omega_c = 520.5$ cm^{-1} frequency phonons, the parameter $L = d/a_0$, d is the diameter, $a_0 = 0.543$ nm is the lattice constant of c-Si, q – the wave vector of the Phonon, is expressed in units ($2\pi/a_0$, and $\omega_c(q) = \omega_c(1 - 0.18q^2)$) the ratio of the dispersion of the phonon in c-Si [13], B is a constant.

Eq. (2) describes the confinement effect (phonon restriction effect) in spherical Si nanocrystals with sizes 1-10 nm [12], while for Raman scattering with large nanoparticles the expression (1) can be used.

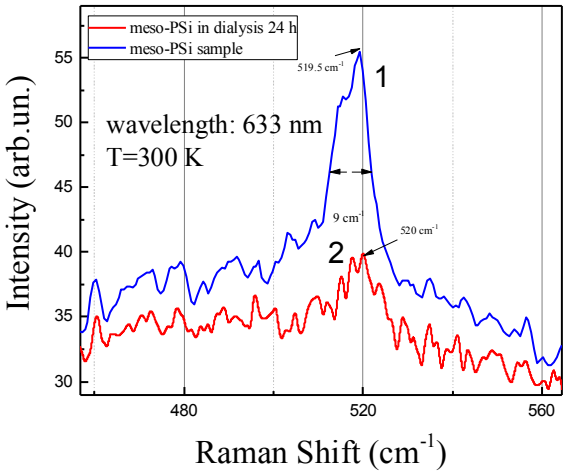

Fig. 2 Raman spectra for the initial meso-PSi (1) sample and after dialysis in water for 24 h (2).

The Raman spectrum of amorphous silicon (a-Si) is described by the following expression [13]:

$$I_A(\omega) = A \times \exp\left(-\frac{(\omega-\omega_a)^2}{2\delta^2}\right), \quad (3)$$

where A is a constant, $\omega_a = 480$ cm^{-1} and $\delta = \Gamma(2\sqrt{2\ln 2})^{-1}$ $\Gamma = 70$ cm^{-1} are the peak position width, respectively.

Assuming that the Raman scattering signal of the sample under study consists of inclusions of all fractions (phases) the forma can be presented as follows:

$$I_{Sum}(\omega) = I_c(\omega) + I_{NC}(\omega) + I_A(\omega). \quad (4)$$

The volume fraction of the nc-Si phase can be calculated as the ratio of the corresponding integrated intensity to the total intensity of the Raman signal:

$$f_{NC} = \int I_{NC}(\omega)d\omega \Big/ \int I_{Sum}(\omega)d\omega. \quad (5)$$

The Raman spectra of meso-PSi analyzed by using Eqs. (1)–(4) show that the average size of Si nanocrystals is about 5 nm and it does not practically change after the storage of the sample in aqueous solution. However, the contribution of the nanocrystalline phase becomes smaller and the signal of a-Si fraction increased (see Fig. 3). The latter indicates an additional disordering of the crystal lattice of NP Si due to their partial dissolution in water in accordance with the findings of Ref. [9].

Investigation of Raman scattering from nonporous nc-Si with sizes from 5 to 100 nm, obtained by plasma chemical (Fig. 3) and laser ablation methods (Fig. 4), indicates partial dissolution of nanoparticles, resulting in a decrease in their total number and average size of nanocrystals. In this case, abl-Si NPs exhibit significantly lower dissolution rate (Fig. 5), compared with NPs obtained by plasma-chemical method that can be explained by a higher concentration of structural defects in the latter.

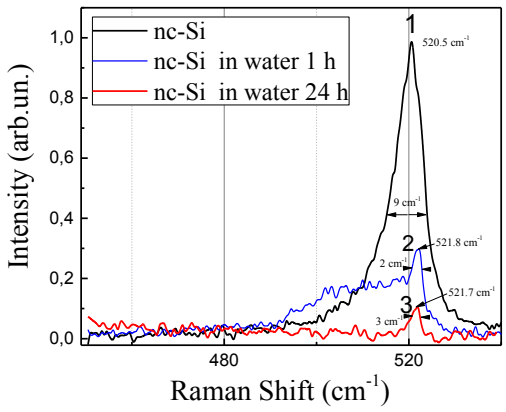

Fig. 3 Raman spectra of nc-Si samples before (1) and after exposure in water for 1 (2) and 24 (3) hours.

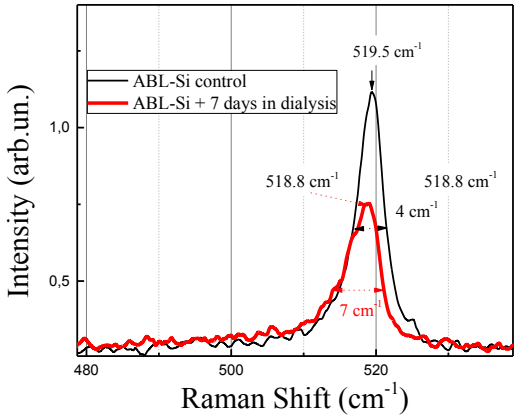

Fig. 4 Raman spectra of abl-Si samples before and after dialysis in water.

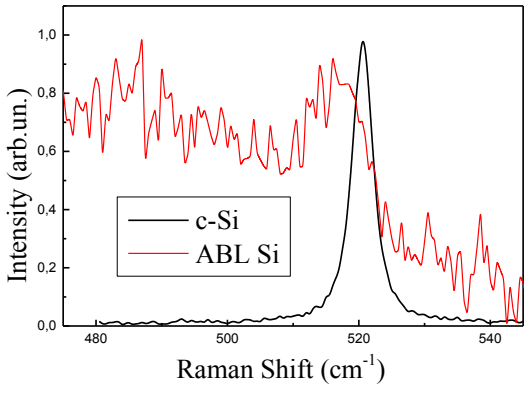

Fig. 5 Raman spectra of aqueous suspension of abl-Si source and c-Si substrate.

The obtained results indicate different dissolution rates of Si nanostructures prepared by wet chemical route and physical methods. Thus, SiNWs, due to their high stability in water, can be used as elements of biosensors. NPs of mesoporous silicon can be

recommended for the purpose of express-diagnostics and therapy, while NPs produced by plasma-chemical synthesis and laser ablation of c-Si in water can be used as agents for short-time and prolonged simultaneous diagnosis and therapy (theranostics) of cancer diseases.

Disclosures

All authors declare that there is no conflict of interests in this paper.

Acknowledgments

The authors thank Prof. A. A. Ishchenko (MIREA – Russian University of technology) for providing the samples obtained by plasma-chemical method, Dr. A.V. Pavlikov for the assistance in selected measurements on the equipment of the Faculty of Physics of Moscow State Lomonosov University.

The work was supported by the state tasks of the Ministry of science and higher education of the Russian Federation (projects 16.2969.2017/4.6 and 16.7917.2017/8.9).

References

1. A. A. Ischenko, G. V. Fetisov, and L. A. Aslanov (eds.), Nanosilicon: Properties, Synthesis, Applications, Methods of Analysis and Control, CRC Press, Taylor& Francis Group, Boca Raton, London, New York (2015).
2. A. V. Kabashin, V. Y. Timoshenko, "What theranostic applications could ultrapure laser-synthesized Si nanoparticles have in cancer?" Nanomedicine 11(17), 2247–2250 (2016).
3. L. A. Osminkina, V. Y. Timoshenko, "Porous Silicon as a Sensitizer for Biomedical Applications: Mini-review," Open Material Sciences 3(1), 39–48 (2016).
4. L. A. Osminkina, A. A. Kudryavtsev, S. V. Zinoviev, A. P. Sviridov, Y. V. Kargina, K. P. Tamarov, V. N. Nikiforov, A. V. Ivanov, A. N. Vasiliev, and V. Y. Timoshenko, "Silicon nanoparticles as amplifiers of ultrasonic action for sonodynamic therapy," Bulletin of experimental biology and medicine 161(2), 296–299 (2016).
5. A. P. Sviridov, L. A. Osminkina, A. L. Nikolaev, A. A. Kudryavtsev, A. N. Vasiliev, and V. Y. Timoshenko, "Lowering of the cavitation threshold in aqueous suspensions of porous silicon nanoparticles for sonodynamic therapy applications," Applied Physics Letters 107(12), 123107 (2015).
6. M. B. Gongalsky, Y. V. Kargina, L. A. Osminkina, A. M. Perepukhov, M. V. Gulyaev, A. N. Vasiliev, Y. A. Pirogov, A. V. Maximychev, and V. Y. Timoshenko, "Porous silicon nanoparticles as biocompatible contrast agents for magnetic resonance imaging," Applied Physics Letters 107(23), 233702 (2015).
7. L. A. Osminkina, A. L. Nikolaev, A. P. Sviridov, N. V. Andronova, K. P. Tamarov, M. B. Gongalsky, A. A. Kudryavtsev, H. M. Treshalina, and V. Y. Timoshenko, "Porous silicon nanoparticles as efficient sensitizers for sonodynamic therapy of cancer," Microporous & Mesoporous Materials 210, 169–175 (2015).
8. S. P. Rodichkina, L. A. Osminkina, M. Isaiev, A. V. Pavlikov, A. V. Zoteev, V. A. Georgobiani, K. A. Gonchar, A. N. Vasiliev, and V. Y. Timoshenko, "Raman diagnostics of photoinduced heating of silicon nanowires prepared by metal-assisted chemical etching," Applied Physics B 121(3), 337–344 (2015).
9. E. Tolstik, L. A. Osminkina, C. Matthäus, M. Burkhardt, K. E. Tsurikov, U. A. Natashina, V. Y. Timoshenko, R. Heintzmann, J. Popp, and V. Sivakov, "Studies of silicon nanoparticles uptake and biodegradation in cancer cells by Raman spectroscopy," Nanomedicine: Nanotechnology, Biology & Medicine 12(7), 1931–1940 (2016).
10. M. B. Gongalsky, L. A. Osminkina, A. Pereira, A. A. Manankov, A. A. Fedorenko, A. N. Vasiliev, V. V.Soloviev, A. A. Kudryavtsev, M. Sentis, A. V. Kabashin, and V. Y. Timoshenko, "Laser-synthesized oxide-passivated bright Si quantum dots for bioimaging," Scientific Reports 6(1), 24732 (2016).
11. A. Kharin, O. Syshchyk, A. Geloen, S. Alekseev, A. Rogov, V. Lysenko, and V. Timoshenko, "Carbon fluoroxide nanoparticles as fluorescent labels and sonosensitizers for theranostic applications," Science and Technology of Advanced Materials 16(4), 044601 (2015).
12. H. Richter, Z. P. Wang, and L. Ley, "The one phonon Raman spectrum in microcrystalline silicon," Solid State Communications 39(5), 625–629 (1981).
13. N. E. Maslova, A. A. Antonovsky, D. M. Zhigunov, V. Y. Timoshenko, V. N. Glebov, and V. N. Seminogov, "Raman studies of silicon eanocrystals embedded in silicon suboxide layers," Semiconductors 44(8), 1040–1043 (2010).
14. A. F. Alykova, I. N. Zavestovskaya, V. G. Yakunin, and V. Y. Timoshenko, "Raman diagnostics of silicon nanocrystals dissolution in aqueous medium," Journal of Physics: Conference Series 945, 012002 (2018).

Estimation of dehydration of skin by refractometric method using optical clearing agents

Ekaterina N. Lazareva[1,2*], Polina A. Dyachenko (Timoshina)[1,2], Alla B. Bucharskaya[3], Nikita A. Navolokin[3], and Valery V. Tuchin[1,2,4,5,6]

[1] Research-Educational Institute of Optics and Biophotonics, Saratov State University, 83 Astrakhanskaya str., Saratov 410012, Russian Federation

[2] Interdisciplinary Laboratory of Biophotonics, Tomsk State University, 36 Lenin Avenue, Tomsk 634050, Russian Federation

[3] Saratov State Medical University, 112 Bolshaya Kazachya str., Saratov 410012, Russian Federation

[4] Laboratory for Laser Diagnostics of Technical and Live Systems, Institute of Precision Mechanics and Control, Russian Academy of Sciences, 24 Rabochaya str., Saratov 410028, Russian Federation

[5] Laboratory of Femtomedicine, ITMO University, 14 Birzhevaya Line, Lit. A., St. Petersburg 197101, Russian Federation

[6] Samara National Research University, 34 Moskovskoye shosse, Samara 343086, Russian Federation

*** e-mail:** lazarevaen@list.ru

Abstract. Optical methods with highly sensitive to water content are important for the development of new diagnostic and therapeutic methods in medicine. The paper presents a quantitative assessment of the dehydration of skin when using optical clearing agents (glycerol and glucose) by the method of multi-wavelength refractometry for the visible and NIR spectral regions. The resulting decrease in the refractive index of the optical clearing solution made it possible to estimate the volume of the fluid extracted from the tissue. The possibility of using the method when conducting *in vivo* measurements is shown. An assessment was made of the degree of dehydration of rat skin in areas with a subcutaneous tumor neoplasm, which was three times less than for control (healthy) skin areas. © 2019 Journal of Biomedical Photonics & Engineering.

Keywords: multi-wavelength refractometry; skin; refractive index; dehydration; optical clearing; glycerol; glucose.

Paper #3317 received 15 Feb 2019; revised manuscript received 26 May 2019; accepted for publication 5 Jun 2019; published online 30 Jun 2019. doi: 10.18287/JBPE19.05.020305.

1 Introduction

Currently, optical methods, such as photoacoustic and terahertz spectroscopy and visualization, and a number of other methods are widely used for the diagnosis and treatment of various diseases [1–9]. The use of optical methods is strongly limited to the small depth of probing tissues [9]. However, when exposed to hyperosmotic optical clearing agents (OCA) on tissue, it is possible to achieve a noticeable decrease in scattering and absorption in water bands in the entire range of working wavelengths due to dehydration of the tissue, respectively, an increase in optical transmission [9–14].

Enhancing image contrast due to dehydration and tissue optical clearing in the area of pathology is extremely important in the diagnosis of precancerous conditions, early stages of cancer and other diseases [1–6, 15–16]. In a number of works, the difference in the content of free and bound water in the tissues was shown and an increased content of free water in the tumor tissues was found [17–20]. It is assumed that protein molecules affect the free water content, which change as a result of the development of pathology. For example, it was shown in Ref. [19] that bound water interacts with the protein and is removed along with it. It should be noted that water is the main absorber in the terahertz frequency range and its reversible removal from tissue contributes to an increase in the depth of sensing of tissues by terahertz radiation [18–21]. The combination of studies in the optical and terahertz ranges opens up new possibilities for a more reliable diagnosis of a number of diseases [22, 23].

Traditional methods for quantifying the dehydration of tissue when exposed to OCA are measurements of changes in weight and geometric parameters [24–26]. However, these methods in practice are applicable only for *in vitro* or *ex vivo* measurements. The refractometric method allows the evaluation of the degree of dehydration for both *in vitro* (*ex vivo*) and *in vivo* measurements. And the measurement of refraction at the same time at several wavelengths makes it possible to obtain more reliable information about the degree of tissue dehydration due to the collection of a larger number of data and rely on determining the composition of the extracted fluid.

In this work, the further development of the refractometric method for estimating the degree of skin dehydration, previously described in Refs. [25, 26], and its application for *in vitro* and *in vivo* studies, which were conducted on laboratory animals with PC1 alveolar liver cancer tumors. *In vitro* measurements using 70% glycerol solution and 40% glucose solution as optical clearing agents were performed on a multi-wavelength Abbe refractometer DR-M2/1550 (Atago, Japan) for wavelengths of 486, 589, 680, 930, and 1300 nm. According to the obtained results, the refractive index of the antireflection solution decreased, which indicated the dehydration of the tissue and allowed a quantitative assessment of the volume of the extracted fluid. As an example, when conducting *in vivo* experiments, skin dehydration was evaluated in areas with a subcutaneous tumor neoplasm and in control (healthy) areas of the skin using the refractometric method for the wavelengths of 480, 486, 546, 589, 644, 656, 680, 800, 930, 1100, 1300, and 1550 nm.

2 Methods and materials

For *in vitro* measurements during the optical clearing experiment, skin samples of healthy laboratory rats were used as samples of the study. Using a micrometer, measurements were made of the thickness, width, and length of the samples before and after the experiment. On an analytical balance (Scientech, SA210, USA) with an accuracy of ±1 mg, the weight of the samples was measured before and after the experiment. Parameters were measured after the experiment and after complete removal of OCA on both sides of the sample.

The samples were placed in a closed sealed container, to which was added 2 ml of OCA. 70% glycerol solution and 40% glucose solution were used with the addition of saline as an OCA. Measurements of the refractive index of OCA were carried out before the start of the experiment and every 5 minutes after placing the skin sample in the solution with OCA for 20 minutes, then every 10 minutes for another 40 minutes. For the measurements, 10 μl of the solution was taken and three samples were taken for each solution.

The refractive index was measured on a multi-wavelength Abbe refractometer DR-M2/1550 (Atago, Japan). The radiation source in this installation is a high power incandescent lamp. For the selection of wavelengths, narrow-band interference filters for 486, 589, 680, 930, 1300 nm were used. The measurement error introduced by the device is ±0.0002. At the beginning of the measurements, the instrument was calibrated against the tabular value of the refractive index of distilled water. The temperature of the measurements during the experiment was 22 °C and was maintained with circulation thermostat.

Evaluation of the degree of dehydration of skin sample was performed using expression of Gladstone-Dale for a multicomponent solution [27, 28]:

$$n(\lambda,t)=\sum_i n_i(\lambda) f_i(t), \tag{1}$$

where n is the refractive index of the solution, i is the number of components of the solution, n_i is the refractive index of the i-th component, f_i is the volume fraction of the i-th component.

Expression (1) in our case will take the form:

$$\begin{aligned} n_{\exp}(\lambda,t) &= n_{OCA}(\lambda) f_{OCA}(t) + n_{NaCl}(\lambda) f_{NaCl}(t) + \\ &+ n_{ext\ fl}(\lambda) f_{ext\ fl}(t), \end{aligned} \tag{2}$$

where $n_{\exp}$ is the refractive index of the experimental solution, n_{OCA} is the OCA refractive index, f_{OCA} is the volume fraction of OCA (glycerol or glucose), n_{NaCl} is the refractive index of saline, f_{NaCl} is the volume fraction of saline solution, $n_{ext\ fl}$ is the refractive index of the extracted fluid, $f_{ext\ fl}$ is volume fraction of the extracted fluid.

From Eq. (2), the refractive index of the OCA is calculated from the measured and known in the literature data for the initial solutions. Initial calculations are performed under the assumption that the refractive index of the extracted fluid is equal to water.

Writing Eq. (2) for the solutions obtained after the enlightenment experiment, the volume fraction of the extracted liquid is calculated from the known data. The expressions for finding the volume fraction of the extracted liquid in glycerol and glucose solutions will be:

$$\begin{aligned} f_{ext\ fl}(t) &= \\ &= \frac{n_{\exp}(\lambda,t) - n_{OCA}(\lambda) + \left(n_{OCA}(\lambda) - n_{NaCl}(\lambda)\right) f_{NaCl}(t)}{\left(n_{ext\ fl}(\lambda) - n_{OCA}(\lambda)\right)}. \end{aligned} \tag{3}$$

The change in the volume fraction of the extracted liquid in the solution of OCA was estimated by the formula:

$$\Delta f = f_{60} - f_0, \tag{4}$$

where f_{60} is the volume fraction of the extracted fluid in the OCA solution after 60 min exposure to the sample,

f_0 is the volume fraction of the extracted fluid in the OCA solution prior to the rat skin clearing experiment.

The found value of the volume fraction of the extracted liquid in the OCA solution was averaged over 5 wavelengths. Since this value is constant for all wavelengths, using also expression (2) one can determine the refractive index of the extracted liquid. Subtract the contribution of water, glycerol and glucose and compare the obtained dispersion dependence with the dispersion of water.

$$n_{ext\ fl}(\lambda) = \frac{n_{\exp}(\lambda,t) - n_{OCA}(\lambda) + n_{OCA}(\lambda) f_{ext\ fl}(t)}{f_{ext\ fl}(\lambda)} + \frac{\left(n_{OCA}(\lambda) - n_{NaCl}(\lambda)\right) f_{NaCl}(t)}{f_{ext\ fl}(\lambda)}, \quad (5)$$

In vivo studies were conducted on two laboratory rats of the Vistar line (sexually mature females weighing 300–400 g). The animal was vaccinated with a tumor, by subcutaneous injection into the area of the scapula by 0.5 ml of 25% tumor suspension of PC1 alveolar liver cancer strain in Hanks solution. Studies were conducted 16 days after injection. For the enlightenment experiment, a solution of glycerol 99.3% was poured into a special cuvette in the amount of 1 ml, which opened part of the skin on the skin to ensure full contact of the OCA with the skin surface for 30 min. After the impact of the OCA, he climbed out of the cell to measure the refractive index. The refractive index of glycerol solutions, as in the experiment described earlier *in vitro*, was measured on an multi-wave Abbe refractometer (Atago, Japan). Interference filters for 480, 486, 546, 589, 644, 656, 680, 800, 930, 1100, 1300, and 1550 nm were used to select wavelengths. Measurements were performed three times for each test solution. The measurement error introduced by the device was ±0.0002. The temperature of the solution during the measurements of the refractive index was 27 °C and was kept constant by means of a circulation thermostat. The volume of the extracted fluid was calculated by the Eq. (3).

3 Results and discussion

The resulting *in vitro* measurements of the dependence of the refractive index of the OCA solution on time are shown in Fig. 1. The approximation of the dependences obtained was performed using the exponential function:

$$y(x) = y_0 + Ae^{Bx}, \quad (6)$$

where y_0, A and B are constant values.

The approximation is shown on the graphs in solid lines.

In Fig. 1, it is noticeable that the refractive index of the 70% glycerol solution decreased more strongly, compared to the refractive index of the 40% glucose solution. It is well known that glycerol is highly viscous and hygroscopic. However, the process of interaction of glycerol with the skin is rather complicated and is not fully understood today, despite the extensive literature on this subject [29]. Due to its high hygroscopicity and high viscosity at relatively short time intervals (1–2 hours), it mainly acts as a hyperosmotic agent, extracting interstitial free and weakly bound water from the tissue, penetrating to the tissue to a lesser extent due to diffusion [14, 30]. Glucose is also one of the common OCA. In Ref. [31], it was shown that the optical clearing when using glucose occurs three times faster than when using glycerol.

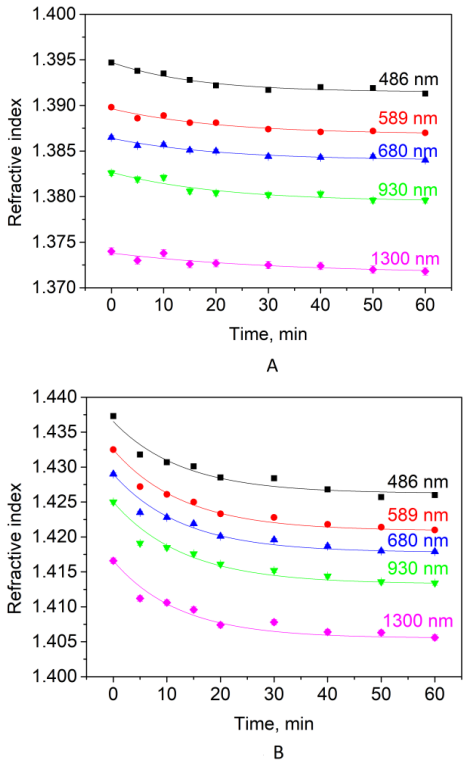

Fig. 1 Dependence of the refractive index of the antireflection solution on time: a) 40% glucose solution; b) 70% glycerol solution.

The measured values of the refractive index according to Eq. (3) were used to calculate the volume fractions of water in the studied solutions for five wavelengths of the visible and near IR regions. The data averaged over five measurements for skin samples and solutions of glucose and glycerol are shown in Table 1 and Table 2.

Fig. 2 shows the increase in the volume fraction of the extracted liquid in a 70% solution of glycerol and a 40% solution of glucose after 60 min of exposure to OCA on a sample of rat skin, calculated by Eq. (4).

In Fig. 2, it can be noted that 70% glycerol solution leads to greater dehydration of the skin compared to 40% glucose solution. The increase in the volume fraction of the extracted liquid in the 70% solution of glycerol was 8.11%, and in the 40% solution of the glucose solution – 2.02%. Due to its high hygroscopicity, glycerol is one of the most effective hyperosmotic OCAs, which confirms our result.

Table 1 Data for skin samples and OCA when exposed to 40% glucose solution.

	Weight sample (mg)	Sample thickness (mm)	Sample length (mm)	Sample width (mm)	The volume of the OCA (ml)	Refractive index	λ (nm)	The volume fraction of water and extracted fluid in the OCA, %	The average volume fraction of water and extracted fluid in the OCA, %
Before exposure to OCA	756±35	1.55±0.20	12.6±0.15	10.05±0.20	2	1.3947±0.0002 1.3898±0.0002 1.3865±0.0002 1.3826±0.0003 1.3740±0.0004	486 589 680 930 1300	60 60 60 60 60	60
After 60 min exposure to OCA	640±25	1.55±0.20	10.50±0.17	7.00±0.18	1.5*	1.3913±0.0002 1.3870±0.0002 1.3840±0.0003 1.3796±0.0003 1.3718±0.0004	486 589 680 930 1300	62.39 62.01 61.80 62.15 61.74	62.02±0.27

* the volume of solution remaining on the sample after it was taken out of solution was not taken into account.

Table 2 Data for skin samples and OCA when exposed to 70% glycerol solution.

	Weight sample (mg)	Sample thickness (mm)	Sample length (mm)	Sample width (mm)	The volume of the OCA (ml)	Refractive index	λ (nm)	The volume fraction of water and extracted fluid in the OCA, %	The average volume fraction of water and extracted fluid in the OCA, %
Before exposure to OCA	805±41	1.55±0.20	12.20±0.20	10.50±0.23	2	1.4373±0.0002 1.4325±0.0002 1.4290±0.0002 1.4250±0.0003 1.4166±0.0003	486 589 680 930 1300	30 30 30 30 30	30
After 60 min exposure to OCA	530±34	1.55±0.20	10.00±0.24	8.10±0.21	1.7*	1.4260±0.0002 1.4210±0.0003 1.4179±0.0002 1.4134±0.0003 1.4056±0.0004	486 589 680 930 1300	37.96 38.16 37.91 38.27 38.26	38.11±0.17

*the volume of solution remaining on the sample after it was taken out of solution was not taken into account.

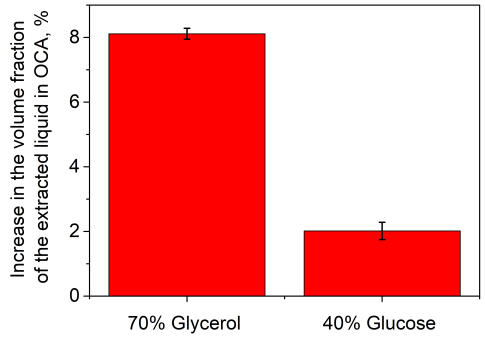

Fig. 2 The change in the volume fraction of the extracted liquid in a 70% solution of glycerol and a 40% solution of glucose after the optical clearing of the sample of rat skin.

Measurement of the refractive index at several wavelengths allowed us the calculation of the dispersion dependence of the refractive index of the extracted substance using Eq. (5) and a comparison with the dispersion of water. Dispersion dependencies for water, 70% glycerol, 40% glucose, and the extracted fluid after skin interaction with glucose and glycerol solutions are shown in Fig. 3.

Presented in Fig. 3, the dispersion curve for the fluid displaced from the skin after exposure to 40% glucose solution is close to the dispersion dependence for water, but larger values of the refractive index for all wavelengths except 486 nm indicate the presence of proteins and salts in the extract. After exposure to 70% glycerol solution, the dispersion is overestimated for all wavelengths in the visible region and coincides with the dispersion of water in the NIR region, which can also be explained by the displacement of intercellular fluid from the tissue, which includes not only water, but also proteins and salts. It can be assumed that the contribution of the protein component is somewhat higher when exposed to glycerol, since protein molecules have a high absorption in the UV region, which leads to a noticeable contribution of anomalous dispersion in UV and corresponding changes in the short-wave visible region due to the wings of the absorption bands.

Table 3 Water content in the glycerol solution after an *in vivo* experiment on clearing of rat skin.

Sample	Volume fraction of glycerol, %	Volume fraction of water, %
Area over healthy tissue	97.0±0.3	3.0±0.3
Tumor area	98.9±0.2	1.1±0.2
Glycerol solution	99.3	0.7

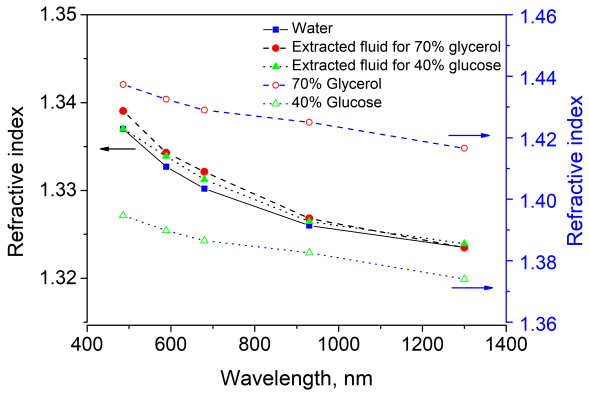

Fig. 3 Dispersion dependencies for water, 70% glycerol, 40% glucose and the isolated fluid after the skin interacts with glucose and glycerol solutions.

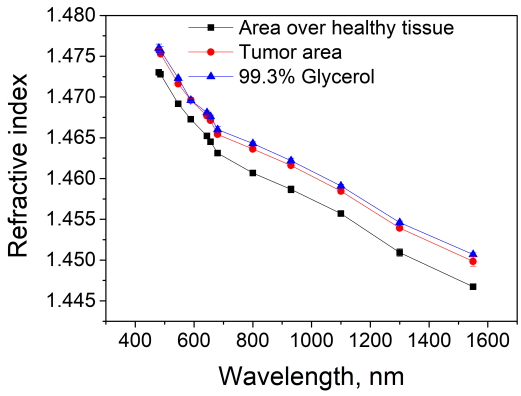

Fig. 4 Dispersion dependence of the refractive index of 99.3% glycerol solution and glycerol solutions after an in vivo experiment on skin on healthy tissue and on a tumor.

Based on the literature data and previously obtained results, the glycerol solution was chosen as an OCA for *in vivo* studies that performed a comparison of the degree of dehydration of tissue in a healthy skin area and in a skin area over a tumor. Based on the obtained values of the refractive index using the Eq. (3), the content of the volume fractions of glycerol and water in the solutions after the *in vivo* experiment was calculated. The obtained volume fractions were averaged for 12 wavelengths for each solution. The data obtained are shown in Figs. 4, 5 and Table 3.

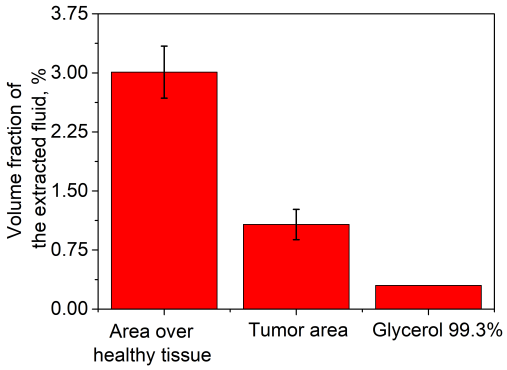

Fig. 5 The volume fraction of water in a glycerol solution after an in vivo experiment on skin areas over healthy tissue and on a tumor, calculated from the refractive index at 12 wavelengths, followed by averaging.

According to the results, the dehydration of a healthy rat skin area was 3.0 ± 0.3%, and for a rat skin area above a tumor it was 1.1 ± 0.2%. This result is generally consistent with the data from the Tromberg group [17], obtained on the basis of spectral measurements for areas of healthy tissue and carcinoma of the female breast, for which the volume of bulk water in healthy tissue was on average 15–16%, and in the tumor about 30%. This, in accordance with the results of [32, 33], means that with a taken concentration of glycerol solution with a water content of 30%, the flow of water extracted from the malignant tissue should be small, while for healthy tissue it is relatively high. Thus, the refractometric method allows one to quickly and simply perform an assessment of the dehydration of the skin in an *in vivo* experiment on optical clearing. The result obtained allows determination of a healthy skin area and a skin area above a tumor, which can be used to develop optical methods for determining the boundaries of a tumor. Also in Fig. 3, it can be noted that for the NIR, the region of the difference in the refractive indices of glycerol solutions after the *in vivo* experiment on areas without a tumor and with a tumor is most noticeable. The difference between the refractive indices of the initial glycerol solution and the refractive index of the glycerol solution after *in vivo* measurements on the skin over healthy tissue is 0.0029 for the visible region (480-680 nm) and 0.0036 for the NIR region (930–1550 nm), and over the tumor, these values are 0.0004 and 0.0007, respectively, can be attributed to the strong contribution of anomalous

dispersion due to water absorption in the NIR of the spectral region.

4 Conclusions

The method of refractometry allows one to quickly and easily to assess the degree of dehydration of tissue when exposed to OCA. Measurements at several wavelengths in the visible and NIR ranges allowed the possibilities of this method to be expanded, including for the analysis of the dispersion curves of the extracted interstitial fluid. The application of the method makes it possible to establish differences in the degree of dehydration for the skin of healthy tissue and a tumor. In the future, the multi-wavelength refractometric method for assessing the degree of dehydration of tissue can be applied to develop new rapid methods for diagnosing and monitoring oncological diseases and increasing the effectiveness of the methods currently used in practice.

Disclosures

All authors declare that there is no conflict of interests in this paper.

Acknowledgments

This work was supported by the RFBR grants 17-00-00275 (K) (17-00-00270 and 17-00-00272) and 18-52-16025.

References

1. E. A. Genina, A. N. Bashkatov, Yu. P. Sinichkin, I. Yu. Yanina, and V. V. Tuchin, "Optical clearing of biological tissues: prospects of application in medical diagnostics and phototherapy," Journal of Biomedical Photonics & Engineering 1(1), 22–58 (2015).
2. A. N. Bashkatov, K. V. Berezin, K. N. Dvoretskiy, M. L. Chernavina, E. A. Genina, V. D. Genin, V. I. Kochubey, E. N. Lazareva, A. B. Pravdin, M. E. Shvachkina, P. A. Timoshina, D. K. Tuchina, D. D. Yakovlev, D. A. Yakovlev, I. Y. Yanina, O. S. Zhernovaya, and V. V. Tuchin, "Measurement of tissue optical properties in the context of tissue optical clearing," Journal of Biomedical Optics 23(9), 091416 (2018).
3. R. Shi, M. Chen, V. V. Tuchin, and D. Zhu, "Accessing to arteriovenous blood flow dynamics response using combined laser speckle contrast imaging and skin optical clearing," Biomedical Optics Express 6(6), 1977–89 (2015).
4. W. Blondel, P. Rakotomanga, G. Khairallah, C. Soussen, W. Feng, D. Zhu, H. Chen, C. Daul, A. Delconte, F. Marchal, and M. Amouroux, "Skin optical properties modifications using optical clearing agents: experimental and modelling results," Presented at International Conference Laser Optics (ICLO), Saint Petersburg, Russia (2018).
5. D. Zhu, K. V. Larin, Q. Luo, and V. V. Tuchin, "Recent progress in tissue optical clearing," Laser & Photonics Reviews 7(5), 732–757 (2013).
6. M. H. Khan, B. Choi, S. Chess, K. M. Kelly, J. McCullough, and J. S. Nelson, "Optical clearing of in vivo human skin: implications for light-based diagnostic imaging and therapeutics," Lasers in Surgery and Medicine 34(2), 83–85 (2004).
7. Y. A. Menyaev, D. A. Nedosekin, M. Sarimollaoglu, M. A. Juratli, E. I. Galanzha, V. V. Tuchin, and V. P. Zharov, "Optical clearing in photoacoustic flow cytometry," Biomedical Optics Express 4(12), 3030–3041 (2013).
8. A. Y. Sdobnov, V. V. Tuchin, J. Lademann, and M. E. Darvin, "Confocal Raman microscopy supported by optical clearing treatment of the skin – influence on collagen hydration," Journal of Physics D: Applied Physics 50(28), 285401 (2017).
9. V. V. Tuchin, Tissue Optics: Light Scattering Methods and Instruments for Medical Diagnostics, 3rd ed., SPIE Press, Bellingham, Washington (2015).
10. D. K. Tuchina, V. D. Genin, A. N. Bashkatov, E. A. Genina, and V. V. Tuchin, Optical clearing of skin tissue ex vivo with polyethylene glycol," Optics and Spectroscopy 120(1), 28–37 (2016).
11. D. K. Tuchina, P. A. Timoshina, V. V. Tuchin, A. N. Bashkatov, and E. A. Genina, "Kinetics of rat skin optical clearing at topical application of 40% glucose: ex vivo and in vivo studies," IEEE Journal of Selected Topics in Quantum Electronics 25(1), 1–8 (2019).
12. W. Feng, R. Shi, N. Ma, D. K. Tuchina, V. V. Tuchin, and D. Zhu, "Skin optical clearing potentialof disaccharides," Journal of Biomedical Optics 21(8), 081207 (2016).
13. L. M. Oliveira, M. I. Carvalho, E. M. Nogueira, and V. V. Tuchin, "Skeletal muscle dispersion (400–1000 nm) and kinetics at optical clearing," Journal of Biophotonics 11(1), e201700094 (2018).
14. E. A. Genina, A. N. Bashkatov, Y. P. Sinichkin, and V. V. Tuchin, "Optical clearing of skin under action of glycerol: ex vivo and in vivo investigations," Optics and Spectroscopy 109(2), 225–231 (2010).
15. W. Feng, R. Shi, N. Ma, D. K. Tuchina, V. V. Tuchin, and D. Zhu, "Skin optical clearing potential of disaccharides," Journal of Biomedical Optics 21(8), 081207 (2016).

16. Z. Zhi, Z. Han, Q. Luo, and D. Zhu, Improve optical clearing skin in vitro with propylene glycol as a penetration enhancer," Journal of Innovative Optical Health Sciences 2(3), 269–278 (2009).
17. S. H. Chung, A. E. Cerussi, C. Klifa, H. M. Baek, O. Birgul, G. Gulsen, S. I. Merritt, D. Hsiang, and B. J. Tromberg, "In vivo water state measurements in breast cancer using broadband diffuse optical spectroscopy," Physics in Medicine and Biology 53(23), 6713–6727 (2008).
18. S. Sy, S. Huang, Y. Wang, J. Yu, A. T. Ahuja, Y. T. Zhang, and E. Pickwell-MacPherson, "Terahertz spectroscopy of liver cirrhosis: investigating the origin of contrast," Physics in Medicine and Biology 55(24), 7587–7596 (2010).
19. S. P. Mickan, J. Dordick, J. Munch, D. Abbott, and X.-C. Zhang, "Terahertz spectroscopy of bound water in nano suspensions," Proceeding of SPIE 4937, 49-61 (2002).
20. A. S. Kolesnikov, E. A. Kolesnikova, A. P. Popov, M. M. Nazarov, A. P. Skurinov, and V. V. Tuchin, "In vitro terahertz monitoring of muscle tissue dehydration under the action of hyperosmotic agents," Quantum Electronics 44(7), 633–640 (2014).
21. G. R. Musina, I. N. Dolganova, K. M. Malakhov, A. A. Gavdush, N. V. Chernomyrdin, D. K. Tuchina, G. A. Komandin, S. V. Chuchupal, O. P. Cherkasova, K. I. Zaytsev, and V. V. Tuchin, "Terahertz spectroscopy of immersion optical clearing agents: DMSO, PG, EG, PEG," Proceeding of SPIE 10800, 108000F (2018).
22. C. S. Joseph, R. Patel, V. A. Neel, R. H. Giles, and A. N. Yaroslavsky, "Imaging of ex vivo nonmelanoma skin cancers in the optical and terahertz spectral regions Optical and Terahertz skin cancers imaging," Journal of Biophotonics 7(5), 295–303 (2014).
23. M. M. Nazarov, O. P. Cherkasova, E. N. Lazareva, A. B. Bucharskaya, N. A. Navolokin, V. V. Tuchin, and A. P. Shkurinov, "A complex study of the peculiarities of blood serum absorption of rats with experimental liver cancer," Optics and Spectroscopy 126(6), 721–729 (2019) [in press].
24. D. K. Tuchina, V. D. Genin, A. N. Bashkatov, E. A. Genina, and V. V. Tuchin, "Optical clearing of skin tissue ex vivo with polyethylene glycol," Optics and spectroscopy 120(1), 28–37(2016).
25. A. N. Bashkatov, E. A. Genina, I. V. Korovina, V. I. Kochubey, Y. P. Sinichkin, and V. V. Tuchin, "In vivo and in vitro study of control of rat skin optical properties by acting of osmotical liquid," Proceeding of SPIE 4224, 300-311 (2000).
26. E. A. Genina, A. N. Bashkatov, I. V. Korovina, Y. P. Sinichkin, and V. V. Tuchin, "Control of skin optical properties: in vivo and in vitro study," Asian Journal of Physics 10(4), 493–501 (2001).
27. R. Barer, "Spectrophotometry of clarified cell suspensions," Science 121(3151), 709–715 (1955).
28. D. W. Leonard, K. M. Meek, "Refractive indices of the collagen fibrils and extrafibrillar material of the corneal stroma," Biophysical Journal 72(3), 1382–1387 (1997).
29. J. W. Wiechers, J. C. Dederen, and A. V. Rawlings, "Moisturization mechanisms: internal occlusion by orthorhombic lipid phase stabilizers – a novel mechanism of skin moisturization," Chap. in Skin Moisturization, A. V. R. Rawlings, J. Leyden (eds.), 2nd edition, Taylor & Francis Group, New York (2009).
30. G. Vargas, E. K. Chan, J. K. Barton, H. G. Rylander III, and A. J. Welch, "Use of an agent to reduce scattering in skin," Lasers in Surgery and Medicine 24(2), 133–141 (1999).
31. R. Cicchi, F. S. Pavone, D. Massi, and D. D. Sampson, "Contrast and depth enhancement in two-photon microscopy of human skin ex vivo by use of optical clearing agents," Optics Express 13(7), 2337–2344 (2005).
32. S. Carvalho, N. Gueiral, E. Nogueira, R. Henrique, L. Oliveira, and V. V. Tuchin, "Glucose diffusion in colorectal mucosa—a comparative study between normal and cancer tissues," Journal of Biomedical Optics 22(9), 091506 (2017).
33. A. Y. Sdobnov, J. Lademann, M. E. Darvin, and V. V. Tuchin, "Methods for Optical Skin Clearing in Molecular Optical Imaging in Dermatology," Biochemistry (Moscow) 84(S1), 144–158 (2019).

Monte Carlo simulation of skin multispectral autofluorescence

Anastasia O. Ustinova, Ivan A. Bratchenko, and Dmitry N. Artemyev*
Samara National Research University, 34 Moskovskoye shosse, Samara 443086, Russia

* **e-mail:** artemev.dn@ssau.ru

Abstract. This work is devoted to the simulation of human skin autofluorescence in different spectral ranges. Analytical review was performed for selecting the main endogenous fluorophores with the greatest contribution to the skin fluorescence: tryptophan, tyrosine, collagen, melanin, elastin, lipofuscin, protoporphyrin IX, NADH, FAD. It was necessary to set parameters for autofluorescence modeling, such as the absorption/emission spectra of fluorophores, molar concentration, molar extinction coefficient, and quantum yield. The six-layer skin model was designed in the TracePro software and autofluorescence was simulated when excited at different wavelengths in the middle UV (270-300 nm), near UV (330-360 nm) and visible (400-450 nm) spectral ranges. The simulation results were compared with the experimental results of other authors. The principal distinctive factor of this work is the simulation of the human skin autofluorescence excited in different spectral ranges.

Keywords: autofluorescence; Monte Carlo modeling; skin model; skin fluorophores; optical diagnostics.

Paper #3326 received 2 May 2019; revised manuscript received 8 Jun 2019; accepted for publication 15 Jun 2019; published online 30 Jun 2019. doi: 10.18287/JBPE19.05.020306.

1 Introduction

Autofluorescence (AF) of the skin is the fluorescent radiation of natural fluorophores inside the tissue excited by absorption radiation with a specific wavelength. Mathematical modeling of AF makes it possible to predict the behavior of real systems and solve design problems without carrying out real experiments [1].

It is possible to reproduce the spectral-optical properties of a biological object in a model experiment. In this case, the model can simulate the spatial structure, composition, and localization of the fluorophores in a real tissue. It is possible to change the parameters of the skin model: the component concentration, the initial radiation conditions, tracking changes in the fluorescence spectra of an object. The method of AF spectroscopy (AFS) is based on the fluorescence spectra registration of endogenous biomarkers. It is known that tumors of the skin, the oral cavity membranes, the gastrointestinal tract, have a number of specific AF spectra, which can be an additional diagnostic parameter for the doctor [2]. However, the AFS method has a number of unresolved problems. Many fluorophores have similar or overlapping absorption and emission spectra, with the result that the tissue fluorescence has a complex spectral composition. In this regard, there is uncertainty with the excitation wavelength and with the emission wavelength for each specific fluorophore [3]. This paper demonstrates the dependences of the shape and intensity of AF spectra by excitation radiation at different wavelengths in three spectral ranges. The aim of this work is AF simulation of human skin model for interpreting experimental spectra (estimating the fluorophores contributions) and assessment of various tissue states (inflammation, neoplasm, etc.).

2 Modeling of light propagation in tissues by Monte Carlo method

The model of radiation propagation in biological tissue was used to describe and predict the effect of fluorophores on the AF signal. Fluorescence simulation was carried out by the Monte Carlo method using the

Table 1 Fluorescent properties of skin components.

Fluorophore	Quantum yield, η_F	Peak of molar extinction, ε_λ [l/mol·cm]	Molar concentration, C_{ab}, [mol/l]
Elastin [8, 11]	0.25	28400	$6\cdot10^{-5}$
Lipofuscin [6, 13]	0.02	11500	10^{-3}
Protoporphyrin IX [6, 14]	0.06	171000	$1.8\cdot10^{-6}$
NADH [8, 12]	0.019	3400	$2\cdot10^{-3}$
FAD [8]	0.03	11300	$5.3\cdot10^{-5}$
Melanin [7]	0.003	2100	$0.88\cdot10^{-2}$
Tyrosine [9]	0.13	1398	$2.5\cdot10^{-4}$
Tryptophan [8, 15]	0.12	5509	$5\cdot10^{-3}$
Collagen [10]	0.3	52940	$1.8\cdot10^{-3}$

TracePro Expert software environment - 6.0.2, which is designed to analyze radiation propagation in optical systems. This method takes into account absorption and scattering throughout the optical path of a photon through a turbid medium.

The Monte Carlo method is a computational method that includes a random sample of a physical quantity. It has become a popular tool for simulating radiation transfer in tissues, since it provides an accurate solution to the problem of radiation transfer in turbid media with a complex structure. The method is able to solve the radiation transfer equation with any required accuracy, if the necessary computing resources are available. For this reason, this method is considered as a gold standard for modeling the light transfer in tissues. The results of Monte Carlo simulations are often used as a reference for testing other less rigorous methods [4].

The optical scheme in the proposed model consists of a laser source, a detector and a six-layer skin model. The source and detector are perpendicular to each other to avoid illumination of the detector channel. The size of the detector was comparable to the size of the object for the efficient registration of the fluorescent signal. The number of incident photons to excite fluorescence in the simulation was 10,000, which led to the generation of more than 10^6 fluorescent photons. For such amount, the correct result was achieved, since with a larger amount the AF spectrum remained almost unchanged. The tracing process at a single excitation wavelength was about 5-6 minutes.

3 Skin model for multispectral AF measurement

The optical properties such as absorption and scattering coefficients, anisotropy coefficient and refractive indices for each skin layer depending on used wavelength were chosen from the book edited by Prof. Tuchin [5]. The model skin area was selected with the size of 40 mm × 40 mm. The thickness of individual skin layers: the stratum corneum – 10 μm, the epidermis – 100 μm, the papillary dermis – 200 μm, the surface plexus of microvessels – 100 μm, the reticular dermis – 600 μm and the deep plexus of the vessels – 200 μm.

Fluorophores were characterized by quantum yield, molar extinction coefficient, and molar concentration, since the absorption and fluorescence intensity mainly depends on these parameters as [5]:

$$I(\lambda) = I_0 \exp(-\mu_a d) = I_0 10^{-\varepsilon_\lambda c_{ab} d}, \quad (1)$$

$$I_F(\lambda) = I_0 [1 - 10^{-\varepsilon_\lambda c_{ab} d}] \eta_F \Omega / 4\pi, \quad (2)$$

where $I(\lambda)$ is the intensity of the transmitted light, I_0 is the intensity of the incident light, μ_a is the absorption coefficient, d is the layer thickness, ε_λ is the molar extinction coefficient, C_{ab} is the molar concentration, η_F is the quantum yield of fluorescence, Ω is the solid angle of isotropic fluorescence registration.

On the base of the analysis of literature data [6-15], we selected components with the maximum values of fluorescent characteristics. The selected fluorophores and their characteristics are presented in Table 1. The parameters were obtained from experimental studies of healthy human skin.

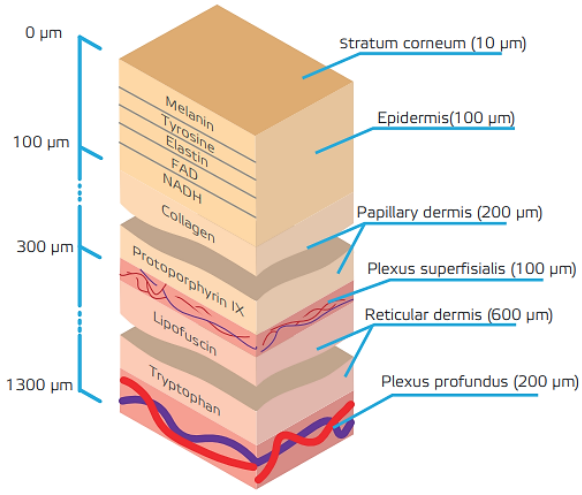

Fig. 1 Fluorophores localization in the six-layer skin model.

The localization of presented fluorophores in the skin model layers was chosen on the basis of papers review [6-15] is shown in Fig. 1. It is important to note that in all spectral ranges, AF modeling was carried out with fixed values of fluorophore concentrations and their location in the human skin model.

Figs. 2 and 3 show the absorption and emission spectra of selected fluorophores. As can be seen from Fig. 2, the absorption spectra can be divided into three ranges. This is due to the fact that the simulation of fluorescence in different spectral ranges makes it possible to carry out a comprehensive analysis of the skin component composition.

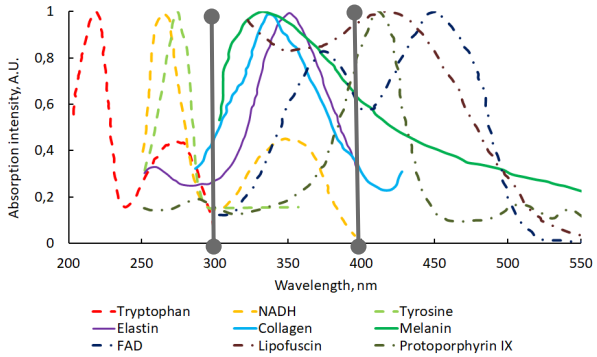

Fig. 2 Absorption spectra of model fluorophores.

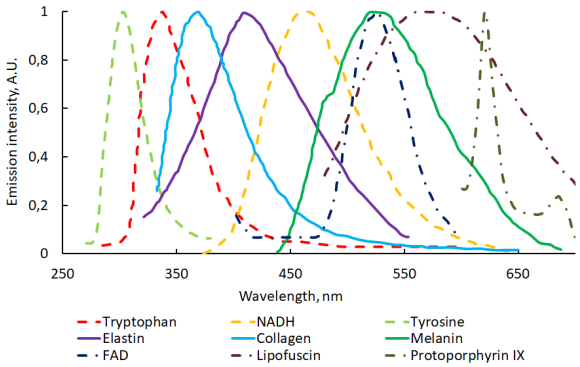

Fig. 3 Emission spectra of model fluorophores.

4 Results and discussion

4.1 Skin model AF excited in the middle UV spectral range (270–300 nm)

The main objective of this work was fluorescence simulation at different wavelengths with appropriate fluorophores. At the first stage, fluorescence was simulated at excitation wavelengths in the middle UV spectral range (270–300 nm). The skin model in this range contained five fluorophores that were excited in the UV range: tyrosine, tryptophan, elastin, NADH, Protoporphyrin IX. The results of skin AF simulating excited by different wavelengths from the mid-UV range are presented in Fig. 4.

The maximum intensity of the AF is observed at a wavelength of 340 nm. This is due to the greatest contribution of tryptophan to the fluorescence spectrum, since at the wavelength of 340 nm there is a fluorescence peak of this component. Although tyrosine at an excitation wavelength of 280 nm has a stronger absorption than tryptophan, but the indicators of the molar extinction coefficient and the molar concentration are significantly lower than that of tryptophan. As the excitation wavelength increases, the absolute values of AF response declines. This is due to the weakening of the emission signals of the fluorophores, which is confirmed by the emission spectra shown in Fig. 3. The fluorescence intensity decreases with increasing excitation wavelength, without changing the shape or shifting the position of the maximum. A decrease of fluorescence upon excitation with radiation at different wavelengths, controlled by the maximum of fluorescent signal was shown in the study by Brancaleon *et al.* [16]. Brancaleon *et al.* obtained similar to our studies results by skin areas irradiating with emitting wavelengths of: 275 nm, 285 nm, 295 nm, 305 nm, and 315 nm.

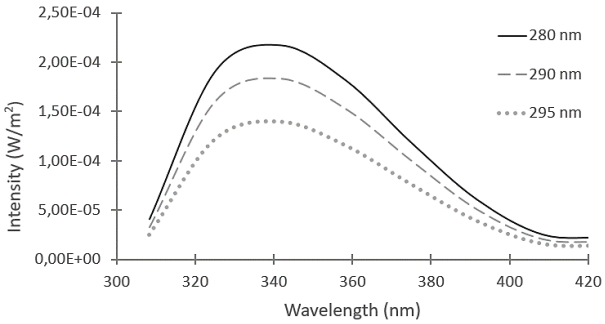

Fig. 4 Model AF spectra of the skin excited by different wavelengths from the mid-UV range.

The efficiency of the model was tested by comparing the simulation results with the experimental data provided by Brancaleon *et al.* [16]. An excitation wavelength of 295 nm was chosen. For comparison, the simulation and experimental fluorescence spectra were normalized to a maximum value of intensity (Fig. 5). This approach was also used to test models in other ranges.

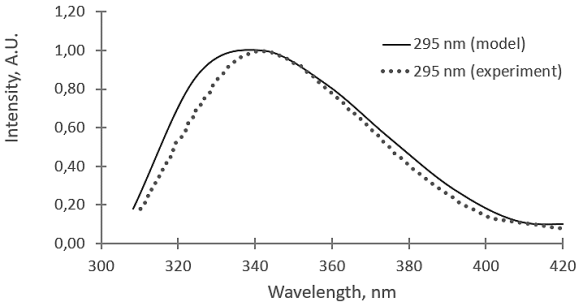

Fig. 5 The simulated and experimental spectra of healthy human skin excited by radiation at wavelength of 295 nm.

Comparing the experimental and modeling spectra reveals small discrepancies with 12% maximum differences. As can be seen from Fig. 5, the

experimental spectrum is shifted to the long-wavelength region. This may be due to the fact that not all amino acids were used in the simulation, but only tyrosine and tryptophan. With a larger number of components of this group, the spectrum should be shifted to the long-wavelength region by the emission contribution of other fluorophores [17].

4.2 Skin model AF excited in the near UV spectral range (330–360 nm)

At the second stage, modeling was performed at excitation wavelengths in the near UV range (330–360 nm). The skin model contained six fluorophores: melanin, elastin, FAD, NADH, collagen, lipofuscin. The skin model fluorescence spectra excited by different wavelengths (337 nm, 350 nm, 360 nm) are presented in Fig. 6.

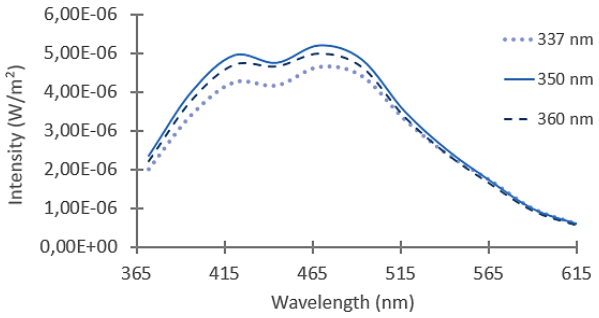

Fig. 6 Model AF spectra of the skin excited by different wavelengths from the near UV range.

The main contribution to the fluorescence spectrum is associated with elastin and FAD. The maximum AF intensity is observed at wavelengths of 415 nm and 490 nm, which correspond to the emission peaks of elastin and FAD, respectively. The emission peak at wavelength of 415 nm is explained by the high value of the elastin absorption coefficient at the excitation wavelength, as well as the high values of the quantum yield and molar extinction coefficient compared to other fluorophores. Melanin also contributes to AF at an emission wavelength of 515 nm, but optical characteristics such as quantum yield and molar extinction coefficient of FAD are several orders of magnitude greater than optical characteristics of melanin.

The model spectrum was compared with experimental results obtained by by Borisova *et al.* [18]. In Fig. 7 we see the coincidence of the main maxima positions and their ratios. An estimate of the difference between the modeled spectrum and the experimental spectrum was also calculated. The difference is 43%. The peak attributable to elastin in the experimental spectrum is located in long wavelength region. This is due to the fact that the simulation did not take into account tryptophan, which could also lead to changes in the AF spectrum. The 450–550 nm range of the simulated spectrum is more stretched compared to the experimental one due to the small number of points taken in the simulation and the components variability.

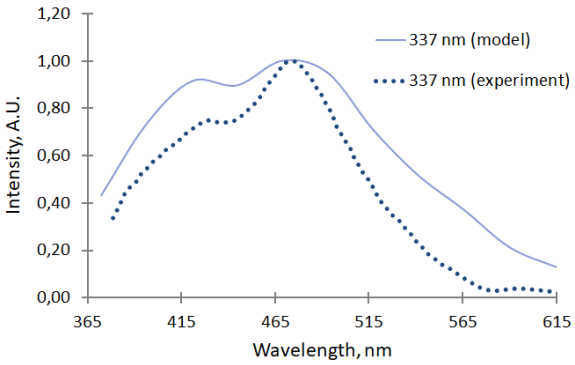

Fig. 7 The simulated and experimental spectra of healthy human skin excited by radiation at wavelength of 337 nm.

4.3 Skin model AF excited in the visible spectral range (400–450 nm)

At the last stage, the fluorescence was simulated in the visible range (380-780 nm) with excitation by radiation with wavelengths of 400-450 nm (Fig. 8). The skin model contained four fluorophores: melanin, FAD, PP IX, lipofuscin.

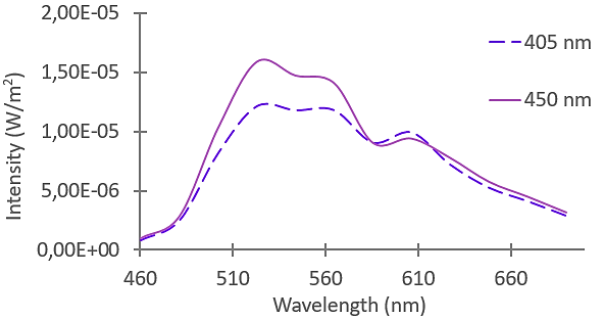

Fig. 8 Model AF spectra of the skin excited by different wavelengths from the visible range.

Peaks of fluorescence are observed at wavelengths of 520 nm, 570 nm and 620 nm. At the peak of 520 nm, FAD makes the largest contribution to AF, since at a given excitation wavelength, this fluorophore has a maximum emission intensity. The peak of the AF spectra at 620 nm is explained by the largest contribution of lipofuscin at an excitation wavelength of 450 nm, since this component has a higher absorption coefficient than FAD. This fact is confirmed by the graph, where there is a change in the ratios of the fluorescence peaks when excited by radiation of 405 nm and 450 nm.

A comparison was also made of the model AF spectrum with the experimental data by Borisova *et al.* upon excitation of skin with 405 nm radiation [18]. Fig. 9 indicates coincidence of the peaks of the modeled and experimental AF spectra, and the difference in

fluorescence intensity is no more than 12%. In this case, the differences in the spectra may be due to the variability of the concentrations of fluorophores and the thicknesses of the skin layers and in different locations.

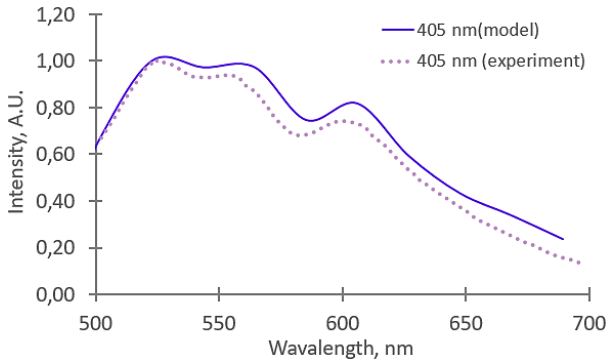

Fig. 9 The simulated and experimental spectra of healthy human skin excited by radiation at wavelength of 405 nm.

5 Conclusion

Monte Carlo simulation was used for modelling of human skin AF spectra. Fluorescence was excited by different wavelengths, a change was observed in the absolute values of the fluorescence intensity (near UV range), as well as the shape of the fluorescence spectra (visible range), which coincides with the experimental data of other authors.

The model fluorescence spectrum excited by radiation in the mid-UV range has minimal differences from the experimental spectrum. It was estimated that this difference is 12%. The AF spectrum when excited in the near UV range, obtained by simulation has a difference of 43%. In the visible range, the difference between the spectra is 12%. The reason for the appearance of differences could be the fact that the simulation of fluorescence in different spectral ranges was carried out with fixed values of the concentrations of fluorophores present in the human skin model and their location. The thickness of human skin and the localization of fluorophores can also vary greatly for different samples of skin and various parts of the body. If necessary, the model can be modified for each specific case and the error of the discrepancy with the experimental data can be reduced to a few percent.

As a result of comparing the AF spectra of healthy human skin in three spectral ranges, obtained by simulation and experiment, it can be concluded that the model is correct and that it is possible to use the proposed model for further research and development. The developed skin model can be used in the analysis (interpretation) of AF experimental data and for the devices design for AF measuring (simulation of various excitation and registration optical schemes).

Disclosures

The author declares that there is no conflict of interests in this paper.

Acknowledgments

This research was supported by the Ministry of Education and Science of the Russian Federation.

References

1. A. C. Croce, G. Bottiroli, “Autofluorescence spectroscopy and imaging: A tool for biomedical research and diagnosis,” European Journal of Histochemistry 58(4), (2014).
2. V. V. Dremin, A. V. Dunaev, “How the melanin concentration in the skin affects the fluorescence-spectroscopy signal formation,” Journal of Optical Technology 83(1), 43–48 (2016).
3. E. G. Borisova, L. P. Angelova, and E. P. Pavlova, “Endogenous and Exogenous Fluorescence Skin Cancer Diagnostics for Clinical Applications,” IEEE Journal of Selected Topics in Quantum Electronics 20(2), 211–222 (2014).
4. P. Meredith, J. Riesz, “Radiative Relaxation Quantum Yields for Synthetic Eumelanin,” Photochemistry and Photobiology 79(2), 211-216 (2004).
5. V. V. Tuchin, Tissue Optics, Light Scattering Methods and Instruments for Medical Diagnostics, Third Edition, SPIE, Bellingham (2007). ISBN: 9781628415162.
6. M. A. Ansari, E. Mohajerani, “Mechanisms of Laser-Tissue Interaction: I. Optical Properties of Tissue,” Journal of Lasers in Medical Sciences 2(3), 119-125 (2011).
7. G. D. Fasman, Handbook of Biochemistry and Molecular Biology, Third Edition, Ohio CRC Press, Cleveland (1976). ISBN 9780367260903.
8. R. F. Chen, “Measurements of absolute values in biochemical fluorescence spectroscopy,” Journal of Research of the National Bureau of Standards Section A: Physics and Chemistry 76A(6), 593-606 (1972).
9. I. Meglinski, Biophotonics for Medical Applications, Elsevier, Amsterdam (2014). ISBN: 9780857096623.
10. Collagen alpha-1(I) chain, Protein A005366, Signaling Gateway (date of access: 29.04.2018).
11. Elastin, Protein A002955, Signaling Gateway (date of access: 29.04.2018).

12. J. Tombran-Tink, C. J. Barnstable, Retinal Degenerations: Biology, Diagnostics, and Therapeutics, Humana Press, Totowa, NJ (2007). ISBN 9781597451864.
13. J. R. Sparrow, Y. Wu, C. Y. Kim, and J. Zhou, "Phospholipid meets all-trans-retinal: the making of RPE bisretinoids," Journal of Lipid Research 51(2), 247–261 (2009).
14. M. Gouterman, G.-E. Khalil, "Porphyrin free base phosphorescence," Journal of Molecular Spectroscopy 53(1), 88-100 (1974).
15. K. S. Brandenburg, K. J. Rodriguez, J. F. McAnulty, C. J. Murphy, N. L. Abbott, M. J. Schurr, and C. J. Czuprynski, "Tryptophan inhibits biofilm formation by Pseudomonas aeruginosa," Antimicrobial Agents and Chemotherapy 57(4), 1921–1925 (2013).
16. L. Brancaleon, G. Lin, and N. Kollias, "The In Vivo Fluorescence of Tryptophan Moieties in Human Skin Increases with UV Exposure and is a Marker for Epidermal Proliferation," Journal of Investigative Dermatology 113(6), 977-982 (1999).
17. D. M. Jameson, "A Fluorescent Lifetime: Reminiscing About Gregorio Weber," Chap in Perspectives on Fluorescence, 1-16 (2016).
18. E. Borisova, P. Pavlova, E. Pavlova, P. Troyanova, and L. Avramov, "Optical Biopsy of Human Skin – A Tool for Cutaneous Tumours' Diagnosis," International Journal Bioautomation 16(1), 53-72 (2012).